Supplementary Information

Meeting U.S. light-duty vehicle fleet climate targets with battery electric vehicles and electrofuels

Dijuan Liang [1], Alexandre Milovanoff [1], Hyung Chul Kim [2], Robert De Kleine [2], James E. Anderson [2], I. Daniel Posen [1], Heather L. MacLean [1]

1: Department of Civil & Mineral Engineering, University of Toronto, Toronto, Canada

2: Research and Innovation Center, Ford Motor Company, Dearborn, MI 48121, United States

Corresponding author: Dijuan Liang, dijuan.liang@mail.utoronto.ca

Table of Contents

1. Introduction

1.1 Literature review of fleet-level studies that included electrofuels (e-fuels)

Table S1 lists studies that evaluated the greenhouse gas (GHG) mitigation potential of e-fuels at the fleet level for light-duty vehicles (LDVs).

Table S1 Review of light-duty vehicle (LDV) fleet-level studies that included electrofuels (e-fuels)

Study	**How the study assessed the mitigation potential of e-fuels and study results**
Searle & Christensen [1]	Estimated supply potential of e-fuels in the European Union (EU) based on cost and deployment rate and projected maximum greenhouse gas reduction of 4 Mt CO_2-eq per year in EU road transport by 2030 under policy support of €3/L.
Rottoli et al. [2] & Dirnachner et al. [3]	Compared greenhouse gas mitigation potential of the large-scale deployment of electric vehicles (EVs) with e-fuels in the European light-duty vehicle (LDV) fleet to meet a global emission budget (800 Gt CO_2, 2011-2100). Both strategies were projected to meet the climate targets but required bioenergy with carbon capture and storage to be deployed to offset emissions from light-duty vehicles, and using e-fuels was shown to have higher impacts on health, ecosystem, and resources.
Rüdisüli et al. [4], [5]	Compared fleet-level greenhouse gas emission reduction and requirements in the energy system from large-scale deployment of battery electric vehicles (BEVs), hydrogen fuel cell electric vehicles, and synthetic natural gas vehicles (SNG-Vs) in the 2015-2050 Swiss passenger car fleet, and reported the lowest emissions from using BEVs if flexibility options are available.
Garcia et al. [5]	Compared fleet-level well-to-wheel greenhouse gas reduction in the EU and U.S. car fleets by the large-scale deployment of EVs versus e-fuels, and found EVs would result in more reduction in EU while e-fuels would result in more reduction in the U.S.
Net Zero America [6]	Devised pathways for reaching net-zero emissions by 2050. For one scenario, e-fuels were assumed to replace all conventional gasoline and diesel. It is unclear whether the upstream emissions (e.g., embodied emissions from renewable electricity generation, vehicle cycle) were included.
Helgeson & Peter [7]	Simulated a cost-minimal decarbonization pathway for the electricity and road transportation sectors in European countries to 2050. Power-to-x gasoline and diesel were included. Unclear whether embodied emissions from renewable electricity generation and vehicle cycle were included.

2. Methods

2.1 Methods of sensitivity analysis on fuel-level GHG emissions

In the default case for mass and energy balance data, we adopt carbon capture data from the Greenhouse Gases, Regulated Emissions, and Energy Use in Transportation (GREET) Model 2022 [8] and other (non-carbon capture) process data from Soler et al. [9]. To evaluate the impact of data source selection, we conduct a sensitivity analysis on fuel-level greenhouse gas (GHG) emissions of e-gasoline using multiple data sources in mass and energy balance for carbon capture and other processes (**Table S2**). For carbon capture data from GREET 2022 [8], we further include two industrial flue gas sources (natural gas combined cycle power plants, ammonia production plants) and three direct air capture (DAC) technologies (low-temperature DAC under current status and future status, and high-temperature DAC). For e-gasoline transportation & distribution (T&D), we adopt the same value (0.01 kg CO_2-eq/kg e-gasoline) from GREET 2022 [8] for all options.

Table S3 lists energy requirements for carbon capture from various data sources, while **Table S4** lists feedstock requirements for the whole e-gasoline production process and energy requirements for e-gasoline production processes other than carbon capture. Emission factors of energy inputs are default values: 438 g CO_2-eq/kWh for the 2022 U.S. grid electricity [8], [10], 39.2 g CO_2-eq/kWh for solar PV electricity [8], 10.4 g CO_2-eq/kWh for wind electricity [8], 75.4 g CO_2-eq/MJ for natural gas heat [11], and 0.251 g CO_2-eq/MJ for solar thermal heat [11].

Table S2 Scenarios and data sources for sensitivity analysis on fuel-level GHG emissions

#	Scenario of fuel-level sensitivity analysis	Data source for stages [1]		
		Carbon capture	Other processes [2]	T&D
1	All default (DAC)	GREET 2022 (LT DAC current)	Soler et al.	GREET 2022
2	All default (IND)	GREET 2022 (NGCC)	Soler et al.	GREET 2022
3	All Hombach (DAC)	Hombach et al.	Hombach et al.	GREET 2022
4	Giesen + Hombach (IND)	Giesen et al.	Hombach et al.	GREET 2022
5	All Soler (DAC, IND)	Soler et al.	Soler et al.	GREET 2022
6	All Ordóñez (DAC, IND)	Ordóñez et al.	Ordóñez et al.	GREET 2022
7	All GREET (DAC)	GREET 2022 (LT DAC current)	GREET 2022	GREET 2022
8	All GREET (IND)	GREET 2022 (NGCC)	GREET 2022	GREET 2022
9	Improved DAC (LT)	GREET 2022 (LT DAC future)	Soler et al.	GREET 2022
10	Improved DAC (HT)	GREET 2022 (HT DAC)	Soler et al.	GREET 2022
11	IND from NH3	GREET 2022 (Ammonia)	Soler et al.	GREET 2022

[1] Five data sources are adopted: Hombach et al. [11], Giesen et al. [12], Soler et al. [9], Ordóñez et al. [11], and GREET 2022 [8].

[2] Other processes include hydrogen production, syngas production (reverse water gas shift reactions or co-electrolysis), and chemical synthesis (Fisher-Tropsch synthesis or methanol synthesis with the

methanol-to-gasoline process), hydro-processing (hydrocracking or hydrotreatment), and product separation & upgrading.
Abbreviations: T&D: transportation and distribution; GREET: Greenhouse Gases, Regulated Emissions, and Energy Use in Transportation Model; IND: CO_2 captured from industrial sources; DAC: direct air capture; LT: low temperature; HT: high temperature; NGCC: natural gas combine cycle.

Table S3 Energy requirements for carbon capture from various sources

#	CO_2 source	Industrial source	Data source [1]	Energy requirements for carbon capture	
				Electricity (kWh/kg CO_2)	External heat (MJ/kg CO_2)
1	Industrial CO_2	Natural gas power plant	Giesen et al. [12]	0.48	0
			GREET 2022 [8]	0.34	0
		Coal power plant	Ordóñez et al. [11]	0	0
		Steam methane reforming	Soler et al. [9]	0.14	ELE: 0 [1] COE: 0.13 [1]
		Ammonia production	GREET 2022 [8]	0.09	0
2	Direct air capture	NA	Hombach et al. [11]	0.38	6.1
		NA	Soler et al. [9]	0.5	ELE: 3.3 [2] COE: 5.0 [2]
		NA	GREET 2022 [8]	LT current: 0.72 LT future: 0.52 HT: 0.26	LT current: 14.88 LT future: 6.75 HT: 8.81

[1] Numbers in the tables correspond to using heat produced from Fischer-Tropsch synthesis in carbon capture. If no heat integration between the two processes is considered, 0.9 MJ of heat/kg CO_2 is needed.

[2] Numbers in the tables correspond to using heat produced from Fischer-Tropsch synthesis in carbon capture. If no heat integration between the two processes is considered, 5.8 MJ of heat/kg CO_2 is needed.

Abbreviation: ELE: electrolysis; COE: co-electrolysis; LT: low temperature; HT: high temperature; NA: not applicable

Table S4 Feedstock requirements for the whole e-gasoline production process and energy requirements for e-gasoline production processes other than carbon capture (CC)

#	E-gasoline production pathway	Data source	Feedstock requirements		Energy requirements (processes other than CC)
			H_2	CO_2	Electricity

			(kg/MJ)	(kg/MJ)	(kWh/MJ)
1	FT-ELE	Hombach et al. [11]	0.01	0.08	0.60
		Ordóñez et al. [11]	0.01	0.10	0.73
		Soler et al. [9]	0.01	0.09	0.60
		GREET 2022 [8]	0.02	0.15	0
2	FT-COE	Hombach et al. [11]	NA	0.08	0.40
		Ordóñez et al. [11]	NA	0.11	0.77
		Soler et al. [9]	NA	0.09	0.51
3	MTG-ELE	Soler et al. [9]	0.01	0.07	0.53

Abbreviations: FT: Fischer-Tropsch; MTG: methanol-to-gasoline; ELE: electrolysis-based production pathway; COE: co-electrolysis-based production pathway; NA: not applicable.

2.2 Calculate well-to-wheel efficiency

Table S5 lists parameters and data sources to calculate the well-to-wheel efficiencies for battery electric vehicles (BEVs), internal combustion engine vehicles using gasoline (ICEVs-G) with e-gasoline, hybrid electric vehicles (HEVs) with e-gasoline, and fuel cell electric vehicles (FCEVs). Although not part of the main paper, we also include FCEVs in our efficiency comparison as they provide an alternate pathway for using H_2 for light-duty vehicle (LDV) transportation. The well-to-wheel (WtW) efficiency consists of well-to-tank efficiency and tank-to-wheel efficiency.

To calculate the well-to-tank efficiency, we consider the energy losses from different stages for different vehicles. For BEVs, the well-to-tank efficiency consists of the efficiency of electricity transmission & distribution and BEV charging. For ICEVs-G or HEVs using e-gasoline, the well-to-tank efficiency consists of the efficiency of electricity transmission & distribution, H_2 production, carbon capture, and e-gasoline production. For FCEVs, the well-to-tank efficiency consists of the efficiency of electricity transmission & distribution and H_2 production. Efficiency data on electricity transmission & distribution is estimated from the average 5% transmission & distribution loss from 2017 to 2021 in the U.S. [13]. BEV charging efficiency is estimated from the 10% energy loss from battery charging [14]. Efficiencies related to chemical conversion (i.e., H_2 production, carbon capture, e-gasoline production) are estimated using the mass and energy balance with the lower heating value (LHV) of H_2 (119.96 MJ/kg) and e-gasoline (30.9 MJ/L) [8]. Energy losses from the transportation and distribution of hydrogen and e-fuel are not considered in the study. Similarly, energy losses from electricity generation are not considered, however, this does not affect the comparison between pathways since all (BEVs, ICEVs with e-fuels, and FCEVs) rely on electricity as the main energy input.

The tank-to-wheel efficiency differs by driving type [14], [15], [16]. The tank-to-wheel efficiencies used in this study are 55% city and 45% highway driving [14], [15], [16]. The tank-to-wheel efficiencies are estimated from energy losses during vehicle driving, which differ across

vehicle technologies. The tank-to-wheel efficiencies for BEVs, ICEVs-G, and HEVs are the average values collected from [14], [15], [16]. For BEVs, accessory losses, electric drive system losses, and auxiliary electrical losses are considered in [14]. For ICEVs and HEVs, engine losses, auxiliary electrical losses, parasitic losses, and drivetrain losses are considered in [15], [16]. Special for BEVs and HEVs, these two vehicle technologies can recover energy from regenerative braking. BEVs can recover approximately 22% of the energy used for charging from regenerative braking [14]. HEVs can recover 5-9% of energy from regenerative braking [15]. For the tank-to-wheel efficiency of FCEV, we adopt the efficiency of Hyundai Nexo Blue (2019) measured by Lohse-Busch et al. [17]. This vehicle model is picked as it is one of the latest models in [17] and its weight (1928 kg) is closer to the FCEVs with conventional materials (1653 kg) in GREET 2022 [8] than the other 2019 models.

Table S5 Parameters and data sources to calculate well-to-wheel efficiency

Vehicle technology	**Well-to-tank efficiency**		**Tank-to-wheel efficiency**
	Stages	**Value**	**Value**
BEV	Electricity transmission & distribution	95% [13]	74% (without regenerative braking) [14] 99% (with regenerative braking) [14]
	BEV charging	90% [14]	
ICEV-G + e-gasoline	Electricity transmission & distribution	95% [13]	20% [16]
	H_2 production, carbon capture, e-gasoline production	27-52% [8], [9]	
HEV + e-gasoline	Electricity transmission & distribution	95% [13]	23% (without regenerative braking) [15] 30% (with regenerative braking) [15]
	H_2 production, carbon capture, e-gasoline production	27-52% [8], [9]	
FCEV	Electricity transmission & distribution	95% [13]	64% [17]
	H_2 production	67% (AEL electrolysis) [11]	

Abbreviations: BEV: battery electric vehicle; ICEV-G: internal combustion engine vehicle using gasoline; HEV: hybrid electric vehicle; FCEV: fuel cell electric vehicle; AEL: alkaline electrolysis.

2.3 Calculate CO_2 emission budgets to meet climate change targets

We quantify cumulative CO_2 emission budgets for the U.S. LDV fleet to meet climate targets using methods developed in our prior work [18], which are based on global carbon emission pathways developed by Integrated Assessment Models (IAMs) [19]. These emission pathways outline potential temporal and spatial distributions of CO_2 emissions consistent with specific climate targets under various shared socio-economic pathways (SSPs). The emission pathways are then downscaled at the national and sectoral levels with an allocation approach. We apply the contraction & convergence approach that shares the GHG emission budget among nations and sectors, while allowing expansions of emissions for the least economically developed nations [20]. To further downscale the budget to the sectoral level, we assume proportional efforts from all sectors, and thus the contributions from life-cycle emissions from the U.S. LDV fleet are assumed to be 29% during 2015-2050. Note that this is higher than the reported share of LDV GHG emissions in national GHG inventories [21], primarily due to the inclusion of life cycle emissions and (to a lesser extent) due to the inclusion of non-CO_2 emissions in the calculation for 2015 LDV emissions (i.e., in the numerator), compared to national CO_2 emissions (the denominator). With six IAMs, four SSPs, and two convergence years (2040 and 2050), we obtained 26 different budgets for the 1.5 °C target and 38 for the 2 °C target, and the median of each distribution is used as default in the analysis [18].

Our budget (33 Gt CO_2) is tighter than the U.S. LDV fleet cumulative CO_2 budget (44-50 Gt CO_2) from 2015 to 2050 under the 2 °C climate targets in [22] due primarily to the different sectoral allocation approaches employed. Milovanoff et al. [22] applied the Global Change Assessment Model (GCAM) to estimate the U.S. LDV fleet CO_2 emission budgets consistent with the 2 °C climate targets under various SSPs, and then adjusted the budgets to the system boundary consistent with the Fleet Life Cycle Assessment and Material-Flow Estimation (FLAME) model . This resulted in a larger-than-proportionate share of the GHG budget being allocated to the LDV fleet. Our BAU emission projection is also lower, due to the lower future vehicle stock (reaching 273 million vehicles in 2050) updated according to Annual Energy Outlook (AEO) 2022 [10]. Although the larger budget may reflect the relative difficulty of decarbonizing mobile emission sources, the proportional allocation we employ is conceptually simpler and is more conservative and robust to exogenous efforts from other sectors.

This study pairs CO_2 emission budgets from the IAMs with GHG emissions (consolidated in CO_2-eq using the 100-year global warming potentials, GWP) from the LDV fleet for the LDV sectoral targets and backcasting analysis. This introduces a minor inconsistency but allows us to remain consistent with climate science (where budgets are generally based specifically on cumulative CO_2) while preventing shifting burdens among different GHGs. We argue this is a reasonable compromise due to the low overall contribution from non-CO_2 GHG emissions in the life cycle of LDVs [23], prior work suggesting that GWP remains a good metric for LDV fleets [23], and the

challenges that would be involved in setting a GHG budget that more directly accounts for non-CO_2 GHG emissions [24].

2.4 Calculate emergence growth rate

2.4.1 Data source

Historical production data on biodiesel and ethanol in the U.S. is collected from the U.S. Energy Information Administration (EIA) [25]. Historical production data on oil refineries from 1949 to 2021 in the U.S. is collected from the bp Statistical Review of World Energy [26]. Production data on oil refineries in 1864, 1865, 1872, 1873, 1881, 1884, 1888, 1895, 1896, 1897, 1906, and 1911 are collected from Williamson et al. [27]. Years with missing values are filled with linear interpolation. Data on unconventional growth is obtained from Odenweller et al. [28].

2.4.2 Calculation methods

Emergence growth rates are calculated according to methods in Odenweller et al. [28]. Data before reaching the maximum value (including the maximum value) is used for the calculation. Data is first normalized by dividing by the maximum value, and then fitted to a standard logistic curve: $C(t) = \frac{C_{max}}{1 + e^{-k(t - t_0)}}$, where C_{max} is the asymptote (i.e., maximum value), k is the growth constant, and t_0 is the inflection point ($C(t_0) = C_{max}/2$). Emergence growth rates are calculated using the formula: $b = e^k - 1$. The self-starting nonlinear least squares logistic model is applied.

2.5 Calculate demand for critical materials from water electrolyzers

2.5.1 Technologies and materials included

Table S6 shows the water electrolysis technologies and critical materials included in the analysis. We consider the three widely studied water electrolysis technologies: alkaline electrolysis (AEL), proton exchange membrane (PEM) electrolysis, and solid oxide electrolysis cells (SOEC) [29].

AEL electrolyzers submerge nickel-based electrodes in an alkaline electrolyte solution (usually potassium hydroxide) and separate electrodes with a diaphragm made from polyphenylene sulfide (PPS) [29], [30]. It is a mature and commercialized technology with a longer lifetime and larger capacity for deployment than the other technologies [29]. Neither the U.S. Department of Energy (DOE) [29] nor Kiemel et al. [30] considered critical material use in AEL, while International Energy Agency (IEA) [31] considered nickel (Ni) and zirconium (Zr) and Koj et al. [32] included Ni, Zr, aluminum (Al), copper (Cu), unalloyed steel, etc. Therefore, for critical materials used in AEL, we include Al and Zr as they are on the critical material list [33] and Ni as it was recommended to be included on the critical material list by the United States Geological

Survey (USGS) in 2021 [33]. Cu and steel are excluded because they are not on the critical material list and were not recommended to be included in the list [33].

PEM electrolyzers use platinum-based cathodes and iridium-based anodes, which are separated by a Nafion ion exchange membrane and a titanium (Ti) bipolar plate [29], [30]. U.S. DOE [29] projected PEM to have the highest market share for hydrogen production for synthetic fuels in the U.S. in 2050. Its capital costs are high due to the use of noble metals such as platinum group metals (PGM) [30]. U.S. DOE [29] included platinum (Pt), iridium (Ir), graphite, Ti, chromium (Cr), Ni, and Al for PEM electrolyzers, reporting high supply chain risks for Pt, Ir, and graphite as their future demands are projected to be higher than their current supplies which highly depend on import. Kiemel et al. [30] selected Pt, Ir, and Ti as critical materials for PEM electrolyzers based on expert workshops. IEA [31] included Pt, Ir, and palladium (Pd) in their analysis. For this study, we include Al, Ir, Pt, and Ti as they are all on the critical material list [33]. Although Pd can replace Pt at the cathode and Pd is more abundant and less expensive than Pt [34], Pt is currently the most common cathode material in PEM and the material intensity of Pt is available in the literature [29], [30], and thus Pd is excluded from the analysis. Graphite is on the critical material list [33] and was rated as a high-risk material for PEM electrolyzers and fuel cells by the U.S. DOE [29]. However, different from PEM fuel cells which widely use graphite in catalyst support, gas diffusion layer, and bipolar plates, PEM water electrolyzers only use graphite in the form of carbon paper in the gas diffusion layer [29], [35]. Neither HyTechCycling [35], IEA [31], nor Kiemel et al. [30] listed graphite as a critical material for PEM water electrolyzers. Without a reliable data source of the material intensity of graphite in PEM water electrolyzers, we exclude graphite from consideration. Cr is on the critical material list [33] and was rated as a moderate-risk material for PEM electrolyzers by the U.S. DOE [29]. However, neither Hytechcycling [35], IEA [31], nor Kiemel et al. [30] listed Cr as a critical material for PEM water electrolyzers. Without a reliable data source of the material intensity of Cr in PEM water electrolyzers, Cr is excluded from the analysis. Ru (ruthenium) is on the critical material list [33] and can be used in the anode as a substitute for Ir [29], [35], [36]. However, as Ir is more commonly used and has higher resistance against corrosion [35], [36], we include Ir and exclude Pd in the analysis.

SOECs use oxide ion-conducting electrolytes that are commonly made from yttria-stabilized zirconia and operate under high temperatures [29], [30]. It is an emerging but promising technology with higher efficiency [29], while it is less mature and has a shorter lifetime due to the quick degradation of metals under high temperatures than other technologies [29], [30]. Lanthanum (La), strontium (Sr), cobalt (Co), iron (Fe), manganese (Mn), yttrium (Y), Zr, Ni, stainless steel, and borosilicate glass were included in the critical material assessment for SOEC by U.S. DOE [29], which projected that Sr and Y would be at high supply risk while Co, Fe, La, Mn, and Ni would be at moderate risk. Kiemel et al. [30] considered Y and scandium (Sc) as

critical materials for SOEC. IEA [31] included Ni, Zr, La, and Y in the analysis. In the SOEC model in Hafele et al. [37], yttria-doped ceria (YDC) was used and YDC contains cerium (Ce). We include Zr, Ir, Ti, Co, Gd, La, Mn, Sm, Sr, and Y as they are all on the critical material list [33]. Ni is also included since it is recommended to be included in the list by the USGS [33]. Fe, stainless steel, and borosilicate glass are excluded as they are not on the critical material list and were not recommended to be included [33], and were not rated as high-risk materials for water electrolyzers and fuel cells in U.S. DOE [29]. As a potential substitute for Y [30], Sc is excluded because the U.S. DOE [29] only considered SOEC made from Y rather than Sc and the material intensity of Sc used in SOEC is not available. Ce is ranked 13 in the critical material analysis conducted by USGS [33]. The SOEC model in U.S. DOE [29] did not include Ce, probably because doped ceria is less common than stabilized zirconia in the oxygen ion conductors for the electrolyte layer [38]. Ce is not considered in our study, given that material intensities from U.S. DOE [29] is adopted to keep consistent with other parameters and neither IEA [31] nor Kiemel et al. [30] selected Ce as a critical material for water electrolysis.

Table S6 Materials and technologies selected for the dynamic material flow analysis (MFA) for water electrolyzers

Material	Water electrolyzer technology		
	Alkaline electrolyzer (AEL)	Proton exchange membrane (PEM)	Solid oxide electrolyzer cell (SOEC)
Aluminum (Al)	✓	✓	
Nickel (Ni)	✓		✓
Zirconium (Zr)	✓		✓
Iridium (Ir)		✓	
Platinum (Pt)		✓	
Titanium (Ti)		✓	
Cobalt (Co)			✓
Gadolinium (Gd)			✓
Lanthanum (La)			✓
Manganese (Mn)			✓
Samarium (Sm)			✓
Strontium (Sr)			✓
Yttrium (Y)			✓

2.5.2 Method framework

Figure S1 illustrates the method framework to estimate the demand for critical materials from water electrolyzers. The method is adapted from [29]. After obtaining the annual demand for e-gasoline in the U.S. LDV fleet to meet climate targets for each e-gasoline and BEV deployment scenario, we estimate the associated demand for H_2 and syngas using feedstock requirements

under production pathway and CO_2 source assumptions. Annual demand for H_2 or syngas for e-gasoline production is then used to estimate the annual installed capacity of water electrolyzers using technology share, capacity factor, and energy efficiency. Annual newly installed capacity and retired capacity of water electrolyzers are estimated based on assumed lifetimes. Demands for newly installed and retired capacity are then used to estimate annual demands for critical materials using material intensity, waste intensity during manufacturing, and material recovery rate after the end of life. The annual and cumulative demands for critical materials are further compared with current U.S. consumption, world production, and world reserves, respectively. The following sections contain details of the main steps.

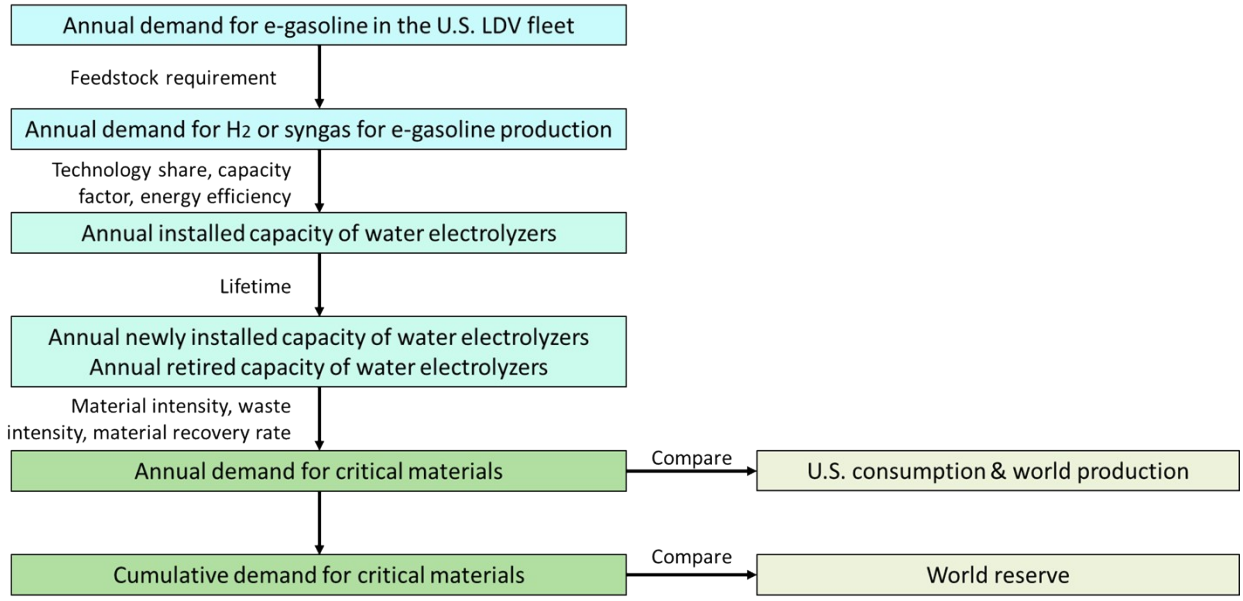

Figure S1 Method flowchart of the dynamic material flow analysis (MFA) to estimate critical material demand in water electrolyzer to produce e-gasoline for the U.S. light-duty vehicle (LDV) fleet

2.5.3 Estimate annual installed capacity

After obtaining the required demand for H_2 and syngas from the FLAME model, we estimate the required annual installed capacity using formula (1), which is adapted from methods in [29].

$$capacity\_ins_{w,t} = \frac{demand\_tot_t \times mar\_share_w \times eff_w}{CF_w \times 365 \times 24 \times 10^3} \quad (1)$$

$$t = 2020,\ldots, 2050; w = AEL, PEM, SOEC$$

$capacity\_ins_{w,t}$ Required installed capacity of technology w in year t, MW

$demand\_tot_t$ Total demand for hydrogen or syngas in year t, $kg\ H_2$ for AEL and PEM, $kg\ syngas$ for SOEC

mar_share_w Market share of technology w

eff_w Energy efficiency of technology w, $\frac{kWh\ electricity}{kg\ H_2}$ for AEL and PEM,

$\frac{kWh\ electricity}{kg\ syngas}$ for SOEC

CF_w Capacity factor of technology w

The market share of technology under various fleet-level scenarios is shown in **Table S7**. We select FT-gasoline as the e-gasoline type since the fuel-level LCAs show that the fuel-level GHG intensities of MTG-gasoline are close to FT-gasoline produced from co-electrolysis-based production pathways. The scenarios are based on using DAC for capturing CO_2 as e-gasoline produced from DAC-based CO_2 is less controversial for assuming carbon-neutral combustion and is more consistent with a future world in which climate targets are being met. DAC is heated by solar thermal energy to ensure that e-gasoline is less GHG-intensive than conventional gasoline.

Scenarios 1 to 6 use one type of technology exclusively to provide upper bounds of estimates on critical material demands. Scenarios 7 to 9 use all types of technology based on the projected market share for all newly installed capacity in the U.S. in 2050 for hydrogen used in synfuels in [29]. As [29] provided market share data only for 2050, we assume that the market share will be constant during the study period. The market share of technology is based on the mass of hydrogen or syngas generation rather than water electrolyzer capacity, consistent with [29].

Table S7 Market share of water electrolyzers under fleet-level scenarios [1]

#	Scenario	Production pathway	Electricity source	Market share of technology		
				AEL	PEM	SOEC
1	All AEL with wind	FT + ELE	Wind	1	0	0
2	All AEL with PV	FT + ELE	Solar PV	1	0	0
3	All SOEC with wind	FT + COE	Wind	0	0	1
4	All SOEC with PV	FT + COE	Solar PV	0	0	1
5	All PEM with wind	FT + COE	Wind	0	1	0
6	All PEM with PV	FT + COE	Solar PV	0	1	0
7	AEL/PEM/SOEC with wind	FT + ELE / COE	Wind	0.2	0.5	0.3
8	AEL/PEM/SOEC with PV	FT + ELE / COE	Solar PV	0.2	0.5	0.3
9	AEL/PEM/SOEC with wind/solar	FT + ELE / COE	Wind / solar PV [2]	0.2	0.5	0.3

[1] All fleet-level FT-gasoline scenarios use CO_2 from direct air capture heated with solar thermal energy and assume the same electricity source for all production steps (i.e., electrolysis / co-electrolysis, carbon capture, syngas production, and Fischer-Tropsch process).

[2] Share of wind and solar electricity source: 44% wind and 56% solar PV (details in SI Section 2.6.3).

Abbreviations: AEL: alkaline electrolysis; PEM: proton exchange membrane electrolysis; SOEC: solid oxide electrolyzer cell; PV: photovoltaic; FT: Fischer-Tropsch; ELE: electrolysis; COE: co-electrolysis.

The values and sources of energy efficiency and capacity are shown in **Table S8**. The capacity factor of 0.9 is used in U.S. DOE [29] under the high capacity factor operation assumption. It is slightly lower than 0.95 for the AEL electrolyzer in Koj et al. [32]. We adopt the value in [29] as it is a more up-to-date report reflecting the U.S. situation and providing numbers for all technologies.

Table S8 Energy efficiency, and capacity factor of water electrolyzers used in this study

Parameter name	Technology	Value	Unit	Source
Energy efficiency	AEL	50	kWh electricity/kg H_2	[9]
	PEM	48	kWh electricity/kg H_2	[39]
	SOEC	7.91	kWh electricity/kg syngas	[9]
Capacity factor	AEL	0.9	NA	[29]
	PEM	0.9	NA	[29]
	SOEC	0.9	NA	[29]

Abbreviations: AEL: alkaline electrolysis; PEM: proton exchange membrane electrolysis; SOEC: solid oxide electrolyzer cell; NA: not applicable.

2.5.4 Estimate annual newly installed and retired capacity

The annual newly installed and retired capacities are estimated using formulas (2)-(4). We assume that both retirement and new installments only occur at the beginning of the year (t). For the starting year 2020, no capacity is assumed to be retired (i.e., $capacity\_ret_{w,\,2020} = 0$, $capacity\_ins\_new_{w,\,2020} = capacity\_ins_{w,\,2020}$). In year t, all capacity installed in previous years (from 2020 to $t-1$) will have certain probabilities of retirement. Therefore, the total retired capacity in t will be the summation of the retired capacity that is installed from 2020 to $t-1$. The capacity that is installed in i and will retire in t can be calculated as the product between the total capacity newly installed in i and the probability that the capacity installed in i would retire in t, i.e., the lifetime of water electrolyzers is $t-i$. Much literature reported lifetime operation hours rather than actual lifetime. Since water electrolyzers are not working full hours across the year (i.e., capacity factor is not equal to 1), the actual lifetime would be longer than the lifetime operation hours. Therefore, we use the capacity factor to obtain the lifetime of water electrolyzers. We assume that the lifetime of water electrolyzers would follow a normal distribution truncated by the minimum lifetime of 1 year and the maximum lifetime from the literature. The maximum lifetime is rounded up to an integer as retirement is assumed to only happen at the beginning of the year and to make sure that the maximum values are used. All values are collected from the literature and some of them are the predicted values for the future (**Table S9**). The lifetime of water electrolyzers is assumed to be unchanged during the study period. Negative values of newly installed capacity are treated as zero and the annual installed capacity is adjusted accordingly.

$$capacity\_ins\_new_{w,\,t} = capacity\_ins_{w,\,t} - capacity\_ins_{w,\,t-1} + capacity\_ret_{w,\,t} \quad (2)$$

$t = 2021,\ldots, 2050; w = AEL, PEM, SOEC$

$capacity\_ins\_new_{w,t}$	Required newly installed capacity of technology w in year t, MW
$capacity\_ins_{w,t}$	Required installed capacity of technology w in year t, MW
$capacity\_ins_{w,t-1}$	Required installed capacity of technology w in year $t-1$, MW
$capacity\_ret_{w,t}$	Capacity of technology w retired in year t, MW

$$capacity\_ret_{w,t} = \sum_{i=2020}^{t-1} capacity\_ret_{w,t}^{i} = \sum_{i=2020}^{t-1} capacity\_ins\_new_{} \quad (3)$$

$$lifetime_w = \frac{lifetime\_oper\_h_w}{365 \times 24 \times CF_w} \sim \mathrm{N}(lifetime\_mean_w, lifetime\_sd_w) \quad (4)$$

$t = 2021,\ldots, 2050; w = AEL, PEM, SOEC$

$capacity\_ret_{w,t}$	Capacity of technology w retired in year t, MW
$capacity\_ret_{w,t}^{i}$	Capacity of technology w that was installed in year i and retired in year t, MW
$capacity\_ins\_new_{w,i}$	Required newly installed capacity of technology w in year i, MW
$lifetime_w$	Lifetime of water electrolyzers in technology w, yr
$lifetime\_oper\_h_w$	Lifetime operation hours of water electrolyzers in technology w, yr
CF_w	Capacity factor of technology w
$lifetime\_mean_w$	Mean of lifetime of water electrolyzers in technology w in the normal distribution, yr
$lifetime\_sd_w$	Standard deviation of lifetime of water electrolyzers in technology w in the normal distribution, yr

Table S9 Lifetime operation hours of water electrolyzers used in the study

Parameter name	Technology	Value	Unit	Source
Mean of lifetime operation hours	AEL	75	1000 hours	[32], [40], [41], [42] [1]
	PEM	50	1000 hours	[29], [41], [42], [43] [1, 2]
	SOEC	22	1000 hours	[29], [41], [42] [1]
Standard deviation of lifetime operation hours	AEL	14	1000 hours	[32], [40], [41], [42] [1]
	PEM	33	1000 hours	[29], [41], [42], [43] [1, 2]
	SOEC	13	1000 hours	[29], [41], [42] [2, 3]
Maximum lifetime operation hours	AEL	100	1000 hours	[41] [3]
	PEM	120	1000 hours	[41] [3]
	SOEC	80	1000 hours	[41] [3]

[1] For IRENA [41], 2020 scenario is adopted.

[2] For Schmidt et al. [42], 2017 scenario is adopted.

[3] For IRENA [41], 2050 scenario is adopted.
Abbreviations: AEL: alkaline electrolysis; PEM: proton exchange membrane electrolysis; SOEC: solid oxide electrolyzer cell.

2.5.5 Estimate annual material demand

Annual demand for critical materials is then estimated using formula (5). Data and sources of material intensity and percentage of material loss during manufacturing are shown in **Table S10** and **Table S11**. Given the high uncertainty of the material recovery rates related to water electrolyzers, we consider two extreme cases to provide upper and lower bounds of estimates: 0% material recovery ($RR = 0$) and 100% material recovery ($RR = 1$). In the 100% material recovery case, materials from both manufacturing waste and retired capacity can be 100% recovered. We only include materials used in stacks and exclude materials used in the balance of plants.

$$demand\_mat_{t,m} = \sum_{w} \{capacity\_ins\_new_{w,t} \times MI_{w,m}[1 + Waste\_perc \quad (5)$$

$$m = Al, Ni, Zr, Ir, Pt, Ti, Co, Gd, La, Mn, Sm, Sr, Y; t = 2020,\ldots, 2050; w = AEL, PEM, SOEC$$

$demand\_mat_{t,m}$	Demand for material m in year t, kg
$capacity\_ins\_new_{w,t}$	Required newly installed capacity of technology w in year t, MW
$MI_{w,m}$	Material intensity of material m for technology w, kg/MW
$Waste\_perc_{w,m}$	Percentage of material loss during manufacturing of material m for technology w
$capacity\_ret_{w,t}$	Capacity of technology w retired in year t, MW
RR	Material recovery rate of material m for technology w

Table S10 Material intensity of water electrolyzers used in the study

Material	Technology	Value	Unit	Source
Aluminum (Al)	AEL	75	kg/MW	[32]
	PEM	27	kg/MW	[43] 2017 scenario
Nickel (Ni)	AEL	3200	kg/MW	[32]
	SOEC	130	kg/MW	[37]
Zirconium (Zr)	AEL	140	kg/MW	[32]
	SOEC	63	kg/MW	[29]
Iridium (Ir)	PEM	1.03	kg/MW	Averages of [41], [43] (today scenario)
Platinum (Pt)	PEM	0.29	kg/MW	Averages of [41], [43] (today scenario)
Titanium (Ti)	PEM	530	kg/MW	[43] 2017 scenario
Cobalt (Co)	SOEC	2.6	kg/MW	[32]

Gadolinium (Gd)	SOEC	0.0048	kg/MW	Transformed from [29]
Lanthanum (La)	SOEC	7.8	kg/MW	Transformed from [29]
Manganese (Mn)	SOEC	1.6	kg/MW	Transformed from [29]
Samarium (Sm)	SOEC	0.0048	kg/MW	Transformed from [29]
Strontium (Sr)	SOEC	2.4	kg/MW	Transformed from [29]
Yttrium (Y)	SOEC	11	kg/MW	Transformed from [29]

Abbreviations: AEL: alkaline electrolysis; PEM: proton exchange membrane electrolysis; SOEC: solid oxide electrolyzer cell

Table S11 Percentage of material loss during manufacturing water electrolyzers used in this study

Material	Technology [1]	Value	Source
Aluminum (Al)	AEL	200%	[8]
	PEM	0%	No data, assume to be 0
Nickel (Ni)	AEL	9%	[8]
	SOEC	19%	[8]
Zirconium (Zr)	AEL	0%	[8]
	SOEC	0%	[8]
Iridium (Ir)	PEM	400%	[8]
Platinum (Pt)	PEM	240%	[8]
Titanium (Ti)	PEM	34%	[8]
Cobalt (Co)	SOEC	20%	[8]
Gadolinium (Gd)	SOEC	0%	[8]
Lanthanum (La)	SOEC	0%	[8]
Manganese (Mn)	SOEC	67%	[8]
Samarium (Sm)	SOEC	0%	No data, assume to be 0
Strontium (Sr)	SOEC	0%	[8]
Yttrium (Y)	SOEC	0%	[8]

Abbreviations: AEL: alkaline electrolysis; PEM: proton exchange membrane electrolysis; SOEC: solid oxide electrolyzer cell.

Much literature reported SOEC material intensities in the form of compound or mixture, and thus we transform the value into the form of the element using chemical formulas in **Table S12**.

Table S12 Chemical formulas for materials used in SOEC used in the study

Abbreviation	Full name	Chemical formula	Source
LSM	Lanthanum strontium manganite	$La_{0.8}Sr_{0.2}MnO_3$	[37]
LSCF	Lanthanum strontium cobalt ferrite	$La_{0.6}Sr_{0.4}Co_{0.8}Fe_{0.2}O_3$	[38] (assume Perovskite-type)
LSM-YSZ	Lanthanum strontium manganite – yttria-stabilized zirconia	50% $La_{0.8}Sr_{0.2}MnO_3$ / 50% $(Y_2O_3)_{0.08}(ZrO_2)_{0.92}$	[44], [45]
8YSZ	8% Yttria-stabilized zirconia	$(Y_2O_3)_{0.08}(ZrO_2)_{0.92}$	[46]

Ni-YSZ	Nickel and yttria-stabilized zirconia ceramic-metal (cermet) composite material	59.34% Ni / 40.66% $(Y_2O_3)_{0.08}$ $(ZrO_2)_{0.92}$	[44], [47]

2.6 Calculate demand for critical materials from renewable electricity generation

2.6.1 Technologies and materials included

Table S13 shows the sub-technologies of onshore wind and solar photovoltaic (PV) technologies and critical materials included in the analysis.

For onshore wind technology, we include six sub-technologies, which can be categorized into two main types: gearbox (GB) and direct drive (DD) [48]. Gearbox configurations can be further divided into designs with double-fed induction generators (DFIG), permanent magnet synchronous generators (PMSG), and squirrel cage induction generators (SCIG) [49]. Gearbox turbines, especially GB-DFIG, are the most widely used onshore wind technology [48], but their heavy weight and high maintenance demand make them less competitive in large-scale deployments [49]. Direct drive configurations can be used with PMSG, electrically excited synchronous generators (EESG), and high-temperature superconductors (HTS). The main strengths of DD-PMSG are the higher efficiency and lower maintenance demand [48], [49]. We include eight materials that are critical to onshore wind technology: aluminum (Al), dysprosium (Dy), manganese (Mn), molybdenum (Mo), neodymium (Nd), nickel (Ni), praseodymium (Pr), and terbium (Tb). Most materials are either included or recommended to be included in the USGS critical material list [33], with the exception of Mo, which is selected as it was included in the critical material assessment by IEA [31].

For solar PV technology, we include four sub-technologies: wafer-based crystalline silicon (c-Si), cadmium telluride (CdTe), copper indium gallium selenide (CIGS), and amorphous silicon (a-Si) [49]. C-Si is currently the dominant sub-technology for solar PV, while the other three sub-technologies (also known as thin-film technologies) are reported to have higher efficiency in absorbing light [49]. We include nine materials that are critical to solar PV technology: aluminum (Al), cadmium (Cd), gallium (Ga), indium (In), selenium (Se), silicon (Si), silver (Ag), tellurium (Te). While many of these materials are on the critical material list [33], Cd, Si, Se, and Ag are not. Cd is considered as it was included in the critical material assessment by IEA [31]. Si was also included in [31] and was rated to be near critical in the medium term by U.S. DOE [48]. Se and Ag were included in the critical material assessment by Carrara et al. [49].

Table S13 Materials and technologies selected for the dynamic material flow analysis for wind power and solar photovoltaic (PV)

Material	Onshore wind [1]	Solar PV [2]

	DD-EESG	DD-HTS	DD-PMSG	GB-DFIG	GB-PMSG	GB-SCIG	c-Si	CdTe	CIGS	a-Si
Aluminum (Al)	✓	✓	✓	✓	✓	✓	✓	✓	✓	✓
Cadmium (Cd)								✓		
Dysprosium (Dy)	✓	✓	✓	✓	✓	✓				
Gallium (Ga)									✓	
Germanium (Ge)										✓
Indium (In)									✓	
Manganese (Mn)	✓	✓	✓	✓	✓	✓				
Molybdenum (Mo)	✓	✓	✓	✓	✓	✓				
Neodymium (Nd)	✓	✓	✓	✓	✓	✓				
Nickel (Ni)	✓	✓	✓	✓	✓	✓				
Praseodymium (Pr)	✓		✓		✓					
Selenium (Se)									✓	
Silicon (Si)							✓			✓
Silver (Ag)							✓			
Tellurium (Te)								✓		
Terbium (Tb)	✓	✓	✓		✓					

[1] Onshore wind sub-technologies can be categorized into two main types: gearbox (GB) and direct drive (DD). Gearbox configurations can be further divided into designs with double-fed induction generators (DFIG), permanent magnet synchronous generators (PMSG), and squirrel cage induction generators (SCIG).

[2] Solar photovoltaic (PV) sub-technologies: wafer-based crystalline silicon (c-Si), cadmium telluride (CdTe), copper indium gallium selenide (CIGS), and amorphous silicon (a-Si).

2.6.2 Method framework

Figure S2 illustrates the framework to estimate the demand for critical materials from onshore wind power and solar PV generation. The method is adapted from Elshkaki & Graedel [50]. After obtaining the annual demand for e-gasoline in the U.S. LDV fleet to meet climate targets for each e-gasoline production and BEV deployment scenario, we estimate the associated demand for electricity based on energy requirements under the production pathway and CO_2 source assumptions. We assume that e-gasoline production facilities would operate continuously with a constant supply of wind and solar electricity, facilitated by the presence of sufficient energy storage. We did not examine critical materials that may be used in energy storage as this was outside of the scope of this study but will be the focus of future work. Annual electricity demand for e-gasoline production is used to estimate annual demand for wind and solar PV power generation with assumed source share, and then to estimate the "ideal" annual installed capacity of wind turbines and solar PV panels by artificially assuming a

capacity factor of 1, which will be adjusted at a later step. The ideal installed capacity is used to estimate the annual newly installed ideal capacity with the lifetime. We then introduce projected real-world capacity factors to adjust (i.e., increase) the required newly installed ideal capacity and later to estimate the demand for newly installed capacity for each sub-technology. The separation of ideal from adjusted (actual) installed capacity adds an extra layer to the procedure, but also creates more flexibility to adjust for future changes in capacity factor. The annual and cumulative demands for critical materials are further estimated and compared using similar methods as water electrolyzers. The following sections explain the formulas and data used in the main steps.

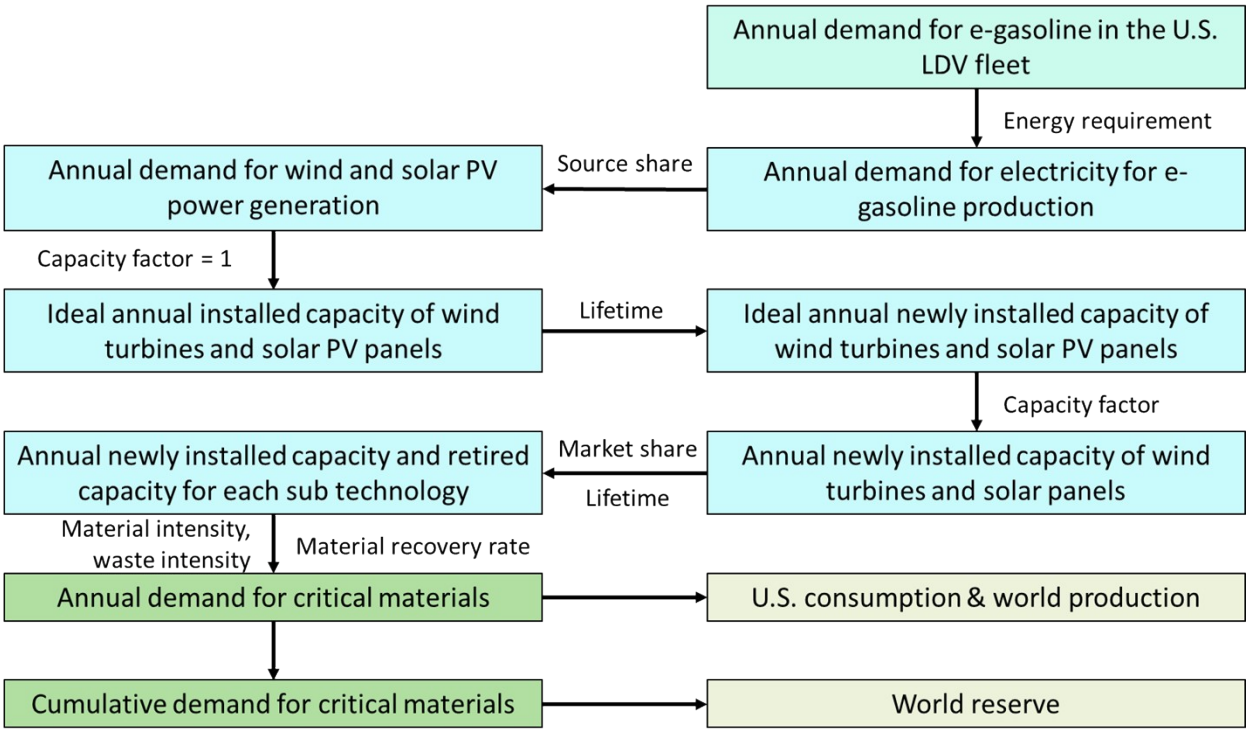

Figure S2 Method flowchart of the dynamic material flow analysis (MFA) to estimate critical material demand from wind and solar PV power generation to produce e-gasoline for the U.S. light-duty vehicle (LDV) fleet

2.6.3 Estimate ideal annual installed capacity

After obtaining the demand for renewable electricity to produce e-gasoline from the FLAME model, we estimate the ideal installed capacity of onshore wind or solar PV by assuming a capacity factor of 1 using formula (6).

$$capacity\_ins\_ideal_{e,t} = \frac{demand\_tot\_ele_t \times source\_share_{e,t}}{365 \times 24} \quad (6)$$

$$t = 2020,\ldots, 2050; e = solar\ PV, wind$$

$capacity\_ins\_ideal_{e,t}$	Required ideal installed capacity of energy source e in year t, kW
$demand\_tot\_ele_{t}$	Total demand for electricity in year t, kWh
$source\_share_{e,t}$	Percentage of electricity that is from energy source e in year t

The source share between onshore wind power and solar PV under various fleet-level scenarios is shown in **Table S14**. We select FT-gasoline produced from CO_2 captured by DAC heated by solar thermal energy and the reasoning has been elaborated in the section on water electrolyzers. Scenarios 1 to 8 use one type of renewable electricity exclusively to provide upper bounds of estimate on critical material demands. Scenario 9 uses both onshore wind power and solar PV electricity based on the projected source share in the AEO 2022 reference case [10]. The dynamic source share in Scenario 9 is only applied for MFA but not for fuel-level GHG emission and e-gasoline demand estimation where constant source share is assumed (44% wind and 56% solar PV).

Table S14 Source share of renewable electricity under various fleet-level scenarios [1]

NO	Scenario	Production pathway	Electricity source	Source share of renewable electricity	
				Onshore wind	Solar PV
1	All AEL with wind	FT + ELE	Wind	1	0
2	All AEL with PV	FT + ELE	Solar PV	0	1
3	All SOEC with wind	FT + COE	Wind	1	0
4	All SOEC with PV	FT + COE	Solar PV	0	1
5	All PEM with wind	FT + COE	Wind	1	0
6	All PEM with PV	FT + COE	Solar PV	0	1
7	AEL/PEM/SOEC with wind	FT + ELE / COE	Wind	1	0
8	AEL/PEM/SOEC with PV	FT + ELE / COE	Solar PV	0	1
9	AEL/PEM/SOEC with wind/solar	FT + ELE / COE	Wind / solar PV	0.797 (2020) – 0.443 (2050)	0.203 (2020) – 0.557 (2050)

[1] All fleet-level FT-gasoline scenarios use CO_2 from direct air capture heated with solar thermal energy and assume the same electricity source for all production steps (i.e., electrolysis / co-electrolysis, carbon capture, syngas production, and Fischer-Tropsch process).
Abbreviations: AEL: alkaline electrolysis; PEM: proton exchange membrane electrolysis; SOEC: solid oxide electrolyzer cell; PV: photovoltaic; FT: Fischer-Tropsch; ELE: electrolysis; COE: co-electrolysis.

2.6.4 Estimate annual newly installed ideal capacity

We estimate the ideal annual newly installed capacity of renewable energy generation following the same approach as water electrolyzers. The lifetime of renewable electricity

generation capacity is assumed to follow Weibull distributions [51], [52] truncated by the minimum lifetime of 1 year and the maximum lifetime in the literature. The values of the parameters are shown in **Table S15**.

Table S15 Lifetime parameters of onshore wind power and solar photovoltaic (PV) used in the study

Parameter name	Energy source	Value	Unit	Source
Scale parameter of lifetime	Onshore wind	19	year	[52]
	Solar PV	30	year	[51]
Shape parameter of lifetime	Onshore wind	4	year	[52]
	Solar PV	10	year	[51]
Maximum lifetime	Onshore wind	35	year	[49]
	Solar PV	30	year	[49]

2.6.5 Adjust to annual newly installed and retired capacity

The ideal annual newly installed capacity is adjusted using the projected real-world capacity factors as shown in formula (7). The annual retired capacity is calculated using the same approach as water electrolyzers.

$$capacity\_new\_adj_{e,t,s} = \frac{capacity\_new\_ideal_{e,t}}{CF_{e,t}} \times mar\_share_{e,t,s} \quad (7)$$

$$t = 2020,\ldots, 2050; e = solar\ PV, wind$$

$$s = \{DD-EESG, DD-PMSG, GB-PMSG, GB-DFIG, GB-SCIG, DD-HTS, c-Si, CdTe, CIGS, a-Si\}$$

$capacity\_new\_adj_{e,t,s}$ Adjusted newly installed capacity of sub-technology s of energy source e in year t, kW

$capacity\_new\_ideal_{e,t}$ Adjusted newly installed capacity of energy source e in year t, kW

$CF_{e,t}$ Capacity factor of energy source e in year t

$mar\_share_{e,t,s}$ Market share of sub-technology s of energy source e in year t

Table S16 shows the capacity factors for onshore wind turbines and solar PV panels in the U.S., which are obtained from the moderate case from the National Renewable Energy Laboratory (NREL) Annual Technology Baseline 2022 [53].

Table S16 Capacity factors for onshore wind and solar photovoltaic used in this study (Source: [53]**)**

Year	Offshore wind	Solar photovoltaic
2020	43.7%	24.4%
2021	44.0%	24.6%
2022	44.4%	24.9%
2023	44.7%	25.1%
2024	45.0%	25.4%

2025	45.4%	25.7%
2026	45.7%	25.9%
2027	46.1%	26.2%
2028	46.4%	26.5%
2029	46.7%	26.7%
2030	47.1%	27.0%
2031	47.1%	27.1%
2032	47.2%	27.2%
2033	47.2%	27.3%
2034	47.3%	27.4%
2035	47.4%	27.5%
2036	47.4%	27.6%
2037	47.5%	27.7%
2038	47.5%	27.8%
2039	47.6%	27.8%
2040	47.6%	27.9%
2041	47.7%	28.0%
2042	47.8%	28.1%
2043	47.8%	28.2%
2044	47.9%	28.3%
2045	47.9%	28.4%
2046	48.0%	28.5%
2047	48.1%	28.6%
2048	48.1%	28.7%
2049	48.2%	28.8%
2050	48.2%	28.9%

Table S17 shows the market share of onshore wind and solar PV technology in 2020 and 2050, which is obtained from the moderate scenario in Carrara et al. [49] for the global market. The values between 2020 and 2050 are linearly interpolated.

Table S17 Market share of onshore wind and solar photovoltaic sub-technologies in 2020 and 2050 used in this study (Source: [49])

Year	Onshore wind						Solar photovoltaic			
	DD-EESG	DD-HTS	DD-PMSG	GB-DFIG	GB-PMSG	GB-SCIG	c-Si	CdTe	CIGS	a-Si
2020	10%	0%	15%	50%	15%	10%	95.4%	2.4%	1.9%	0.3%
2050	0%	0%	25%	40%	25%	10%	90.0%	4.5%	4.5%	1.0%

Abbreviations: DD-EESG: direct-drive with electrically excited synchronous generators; DD-HTS: direct-drive with high-temperature superconductors; DD-PMSG: direct-drive with permanent magnet

synchronous generators; GB-DFIG: gearbox with double-fed induction generators; GB-SCIG: gearbox with squirrel cage induction generators; GB-PMSG: gearbox with permanent magnet synchronous generators; c-Si: wafer-based crystalline silicon; CdTe: cadmium telluride; CIGS: copper indium gallium selenide; a-Si: amorphous silicon.

2.6.6 Estimate annual material demand

The annual demand for critical materials is estimated using the same approach as water electrolyzers. **Table S18** shows the values of material intensity collected from Carrara et al. [49]. For waste intensity, we obtain the fabrication resource efficiencies from Wang et al. [54] (90% for wind turbines and 99% for solar cells), which are transformed into the waste intensity of 11% for wind turbines and 1% for solar panels.

Table S18 Material intensity of onshore wind power and solar PV used in the study (Source: [49]**)**

Material	Energy source	Sub-technology	Value	Unit
Aluminum (Al)	Onshore wind	DD-EESG	700	t/GW
		DD-HTS	700	t/GW
		DD-PMSG	500	t/GW
		GB-DFIG	1400	t/GW
		GB-PMSG	1600	t/GW
		GB-SCIG	1400	t/GW
	Solar PV	c-Si	7200	t/GW
		CdTe	7200	t/GW
		CIGS	7200	t/GW
		a-Si	7200	t/GW
Cadmium (Cd)	Solar PV	CdTe	27	t/GW
Dysprosium (Dy)	Onshore wind	DD-EESG	6	t/GW
		DD-HTS	2	t/GW
		DD-PMSG	17	t/GW
		GB-DFIG	2	t/GW
		GB-PMSG	6	t/GW
		GB-SCIG	2	t/GW
Gallium (Ga)	Solar PV	CIGS	2.5	t/GW
Germanium (Ge)	Solar PV	a-Si	27	t/GW
Indium (In)	Solar PV	CIGS	10	t/GW
Manganese (Mn)	Onshore wind	DD-EESG	790	t/GW
		DD-HTS	790	t/GW
		DD-PMSG	790	t/GW
		GB-DFIG	780	t/GW
		GB-PMSG	800	t/GW
		GB-SCIG	780	t/GW
Molybdenum	Onshore wind	DD-EESG	109	t/GW

(Mo)		DD-HTS	109	t/GW
		DD-PMSG	109	t/GW
		GB-DFIG	99	t/GW
		GB-PMSG	119	t/GW
		GB-SCIG	99	t/GW
Neodymium (Nd)	Onshore wind	DD-EESG	28	t/GW
		DD-HTS	12	t/GW
		DD-PMSG	180	t/GW
		GB-DFIG	12	t/GW
		GB-PMSG	51	t/GW
		GB-SCIG	12	t/GW
Nickel (Ni)	Onshore wind	DD-EESG	340	t/GW
		DD-HTS	340	t/GW
		DD-PMSG	240	t/GW
		GB-DFIG	430	t/GW
		GB-PMSG	440	t/GW
		GB-SCIG	430	t/GW
Praseodymium (Pr)	Onshore wind	DD-EESG	9	t/GW
		DD-PMSG	35	t/GW
		GB-PMSG	4	t/GW
Selenium (Se)	Solar PV	CIGS	20	t/GW
Silicon (Si)	Solar PV	c-Si	2750	t/GW
		a-Si	100	t/GW
Silver (Ag)	Solar PV	c-Si	6	t/GW
Tellurium (Te)	Solar PV	CdTe	27	t/GW
Terbium (Tb)	Onshore wind	DD-EESG	1	t/GW
		DD-HTS	1	t/GW
		DD-PMSG	7	t/GW
		GB-PMSG	1	t/GW

Abbreviations: DD-EESG: direct-drive with electrically excited synchronous generators; DD-HTS: direct-drive with high-temperature superconductors; DD-PMSG: direct-drive with permanent magnet synchronous generators; GB-DFIG: gearbox with double-fed induction generators; GB-SCIG: gearbox with squirrel cage induction generators; GB-PMSG: gearbox with permanent magnet synchronous generators; c-Si: wafer-based crystalline silicon; CdTe: cadmium telluride; CIGS: copper indium gallium selenide; a-Si: amorphous silicon.

2.7 Compare demand for critical materials with current consumption and reserve

Annual demands for critical materials are compared with current U.S. consumption (apparent) and world production, while the cumulative demands are compared with the current world

reserve. Most data are obtained from the USGS Mineral Commodity Summaries 2022 [55]. Detailed data and sources for comparison are shown in **Table S19**. Extra calculations are required to obtain world reserve data for Al and some rare-earth elements (REEs) including Gd, La, Pr, Sm, and Tb. For Al, we obtain the world reserve data of bauxite from USGS [55] (32000 Mt) and the data of hydrated aluminum oxide content in bauxite ore from Natural Resources Canada [56] (50%) to estimate Al world reserve, assuming bauxite ore is the only source for Al. For REEs, we obtain the regional reserve data of rare-earth oxides (REO) from USGS [55] and REO content data for major mines from Mineral Yearbook 2019 [57] to estimate the world reserve of Gd, La, Pr, Sm, and Tb.

Table S19 U.S. apparent consumption, world production, and world reserve data for critical materials

Material	Metric	Year	Value (Mt)	Source
Silver (Ag)	U.S. consumption	2021	0.008	USGS [55]
	World production	2021	0.024	USGS [55]
	World reserve	2021	0.53	USGS [55]
Aluminum (Al)	U.S. consumption	2021	4.3	USGS [55]
	World production	2021	68	USGS [55]
	World reserve	2021	7200	Estimated from USGS [55]
Cadmium (Cd)	U.S. consumption	NA	NA	NA
	World production	2021	0.024	USGS [55]
	World reserve	NA	0.5	Dominish et al. [58]
Cobalt (Co)	U.S. consumption	2021	0.0067	USGS [55]
	World production	2021	0.17	USGS [55]
	World reserve	2021	7.6	USGS [55]
Dysprosium (Dy)	U.S. consumption	NA	NA	NA
	World production	NA	0.0018	Dominish et al. [58]
	World reserve	NA	1.1	Dominish et al. [58]
Gallium (Ga)	U.S. consumption	2021	1.6×10^{-5}	USGS [55]
	World production	2021	4.3×10^{-4}	USGS [55]
	World reserve	NA	0.11	Dominish et al. [58]
Gadolinium (Gd)	U.S. consumption	NA	NA	NA
	World production	NA	0.0075	Emsley [59]
	World reserve	2021	1.72	Estimated from USGS [55] and Mineral Yearbook 2019 [57]
Indium (In)	U.S. consumption	2021	1.7×10^{-4}	USGS [55]
	World production	2021	9.2×10^{-4}	USGS [55]
	World reserve	NA	0.02	Dominish et al. [58]
Iridium (Ir)	U.S. consumption	2021	2.5×10^{-6}	USGS [55]: imports for consumption; 100% reliant on import [29]; assume 1 t of

				platinum-group metals is equal to 1 t of Ir
	World production	2019	8.2×10^{-6}	Mineral Yearbook 2019 [60]
	World reserve	NA	0.0015	Hughes et al. [61]
Lanthanum (La)	U.S. consumption	2019	0.0010	Mineral Yearbook 2019: import data for lanthanum oxide and lanthanum carbonates mixture; no available export data; 100% reliant on import [29]
	World production	NA	0.026	Emsley [59]
	World reserve	2021	25	Estimated from USGS [55] and Mineral Yearbook 2019 [57]
Lithium (Li)	World reserve	2021	22	USGS [55]
Manganese (Mn)	U.S. consumption	2021	0.64	USGS [55]
	World production	2021	20	USGS [55]
	World reserve	2021	1500	USGS [55]
Molybdenum (Mo)	U.S. consumption	2021	0.013	USGS [55]
	World production	2021	0.3	USGS [55]
	World reserve	2021	16	USGS [55]
Neodymium (Nd)	U.S. consumption	NA	NA	NA
	World production	NA	0.016	Dominish et al. [58]
	World reserve	NA	12.8	Dominish et al. [58]
Nickel (Ni)	U.S. consumption	2021	0.21	USGS [55]
	World production	2021	2.7	USGS [55]
	World reserve	2021	95	USGS [55]
Praseodymium (Pr)	U.S. consumption	NA	NA	NA
	World production	NA	NA	NA
	World reserve	2021	4.8	Estimated from USGS [55] and Mineral Yearbook 2019 [57]
Platinum (Pt)	U.S. consumption	2021	3.7×10^{-5}	USGS [55]
	World production	2021	1.8×10^{-4}	USGS [55]
	World reserve	NA	0.03	Hughes et al. [61]
Selenium (Se)	U.S. consumption	2021	4.4×10^{-4}	USGS [55]
	World production	2021	0.003	USGS [55]
	World reserve	2021	0.1	USGS [55]
Silicon (Si)	U.S. consumption	2021	0.46	USGS [55]
	World production	2021	8.5	USGS [55]
	World reserve	NA	NA	NA
Samarium (Sm)	U.S. consumption	NA	NA	NA
	World production	NA	0.0011	Emsley [59]

	World reserve	2021	1.9	Estimated from USGS [55] and Mineral Yearbook 2019 [57]
Strontium (Sr)	U.S. consumption	2021	0.0048	USGS [55]
	World production	2021	0.36	USGS [55]
	World reserve	NA	NA	NA
Terbium (Tb)	U.S. consumption	NA	NA	NA
	World production	NA	NA	NA
	World reserve	2021	0.25	Estimated from USGS [55] and Mineral Yearbook 2019 [57]
Tellurium (Te)	U.S. consumption	NA	NA	NA
	World production	2021	5.8×10^{-4}	USGS [55]
	World reserve	2021	0.031	USGS [55]
Titanium (Ti)	U.S. consumption	NA	NA	NA
	World production	2021	0.21	USGS [55]
	World reserve	2021	449	USGS [55]
Yttrium (Y)	U.S. consumption	2021	5.5×10^{-4}	USGS [55]
	World production	2021	0.009	USGS [55]
	World reserve	2021	0.36	USGS [55]
Zirconium (Zr)	U.S. consumption	2021	0.022	USGS [55]
	World production	2021	0.89	USGS [55]
	World reserve	2021	52	USGS [55]

Abbreviations: NA: no available data.

2.8 Collect production cost and carbon abatement costs of FT-fuels and MTG-gasoline from literature

2.8.1 Literature and boundaries

We collect cost-related results from seven studies (**Table S20**), which estimated and forecasted production costs of FT-fuels (FT-gasoline or FT-diesel) or MTG-gasoline from 2015 to 2050 in various regions. The production cost estimates had different boundaries across studies, but they all included major stages (i.e., electricity generation, H_2 production, CO_2 capture, chemical synthesis, hydrocracking). The stages that are not considered by all studies are H_2 storage & transportation, CO_2 liquefication & storage & transportation, upgrading, byproduct selling, fuel transportation & distribution, and refueling. Five studies in the selected literature estimated GHG emissions (used in assessing abatement costs internally consistent with each source). The boundaries included all major stages but differed in whether construction and demolition of infrastructure and credits for byproduct production were included. The variations in boundaries are expected to impact the comparability of results across studies.

Table S20 Information of literature sources for cost

Source	Region	Timefra	E-fuel	Cost estimate	GHG emission

			me	type	boundary	boundary
1	Soler et al. [9]	Central Europe	2020-2050	FT-diesel, MTG-gasoline	Included: Electricity generation; H_2 production & storage; CO_2 capture & liquefication & storage; chemical synthesis; hydrocracking; upgrading, fuel transportation; refueling	Cradle-to-grave (includes plant maintenance and parts replacement; emissions from plant infrastructure)
2	Hombach et al. [11]	Germany	2015-2030	FT-diesel	Included: Electricity generation; H_2 production & storage; CO_2 capture; chemical synthesis; hydrocracking; upgrading; fuel transportation; refueling	Well-to-wheel (excluded construction of production and distribution infrastructure)
3	Ordóñez et al. [39]	United Kingdom	2018	FT-gasoline	Included: Electricity generation; H_2 production & storage; CO_2 capture; chemical synthesis; hydrocracking; upgrading; byproduct selling Unsure [1]: H_2 transportation; CO_2 liquefication & storage; CO_2 transportation	Cradle-to-gate (included credits from carbon capture)
4	Kannangara et al. [62]	Canada	2019	FT-diesel	Included: Electricity generation; H_2 production; CO_2 capture; chemical synthesis; hydrocracking; upgrading	Cradle-to-grave (included plant construction, end-of-life carbon footprint, credit for carbon capture, credit for gasoline and kerosene production)
5	Ueckerdt et al. [63]	Europe	2020-2050	E-gasoline	Included: Electricity generation; H_2	Cradle-to-grave Unsure: emissions

					production & storage & transportation; CO_2 capture; chemical synthesis; byproduct selling; fuel transportation; refueling Unsure [1]: CO_2 liquefication & storage; CO_2 transportation; hydrocracking; upgrading	related to infrastructure
6	Brynolf et al. [64]	NA	2015-2030	FT-liquids, MTG-gasoline	Included: Electricity generation; H_2 production; CO_2 capture; chemical synthesis; hydrocracking; byproduct selling Unsure [1]: H_2 transportation; CO_2 liquefication & storage	NA
7	Zang et al. [65]	U.S.	Assume 2020	FT-diesel	Included: Electricity generation; H_2 production; CO_2 capture; chemical synthesis; hydrocracking; upgrading Unsure [1]: H_2 storage; H_2 transportation; CO_2 liquefication & storage; CO_2 transportation	NA

[1] Unsure: unsure from the source text whether certain stages were included or not.

Abbreviations: FT: Fischer-Tropsch; MTG: methanol-to-gasoline; NA: not applicable or data unavailable.

2.8.2 Adjust to USD2022

Since different studies used different currencies and nominal values in different monetary years, we adjust all monetary values into U.S. dollars in 2022 (USD2022) using purchasing power parity (PPP) and consumer price index (CPI). PPPs are the rates that reflect the differences in

the purchasing power of different currencies and thus can be used to remove price differences between countries in certain years [66]. CPIs are indexes that reflect the differences in the price of goods and services that households consume over time and thus can be used to remove the price differences within a country over time [67]. Therefore, we first adjust all monetary values to U.S. dollars for each monetary year with PPPs and then transform the results into U.S. dollars in the year 2022 with CPIs, shown in formula (8). Data on both PPP and CPI are collected from the Organisation for Economic Co-operation and Development (OECD) for the Euro area (19 countries) and the U.S. (**Table S21**) [68], [69]. All studies except Ueckerdt et al. [63] specified the monetary year, so we assume its monetary year to be 2020, one year before its publication.

$$real\_val_{USD,2022} = nomi\_val_{cur,t} \times \frac{1}{PPP_{cur,t}} \times \frac{CPI_{USD,\,2022}}{CPI_{USD,t}} \quad (8)$$

$$t = 2015 - 2022$$

$real\_val_{USD,2022}$	Real value in U.S. dollars in year 2022
$nomi\_val_{cur,t}$	Nominal value in currency cur in year t
$PPP_{cur,t}$	PPP of currency cur in year t in the unit of U.S. dollars
$CPI_{USD,\,2022}$	CPI of U.S. dollars in year 2022
$CPI_{USD,t}$	CPI of U.S. dollars in year t

Table S21 Purchasing power parity (PPP) and consumer price index (CPI) used to adjust monetary values

Year	**PPP of Euro (Source:** [68])	**CPI of USD (Source:** [69])
2015	0.755	100
2016	0.730	101
2017	0.721	103
2018	0.713	106
2019	0.695	108
2020	0.692	109
2021	0.699	114
2022	0.684	123

2.8.3 Production cost

We collect production costs of e-fuels from the above studies and use the reported energy density to transform the unit between cost per MJ of fuel and cost per L of fuel. For studies that did not specify the energy density of e-fuels (Kannangara et al. [62], Ueckerdt et al. [63], and Brynolf et al. [64]), the energy density of 30.9 MJ/L from GREET 2022 [8] is used for transformation.

The production costs of conventional gasoline and diesel are approximated by the summation of crude oil price and refinery cost using the historical pump component data. The calculation follows formula (9), which removes taxes and costs for distribution & market price from the retail price. Data on the monthly retail price and component percentage for conventional gasoline and diesel during 2018-2022 is obtained from the U.S. EIA [70], [71].

$$prod\_cost_{f,m,t} = retail\_price_{f,m,t} \times (perc\_crude_{f,m,t} + perc\_refine_{f,m,t}) \quad (9)$$

$$f = gasoline,diesel; m = Jan,\ldots, Dec; t = 2015 - 2022$$

$prod\_cost_{f,m,t}$	Production cost of conventional fuel f in month m in year t
$retail\_price_{f,m,t}$	Retail price of conventional fuel f in month m in year t
$perc\_crude_{f,m,t}$	Percentage of crude oil price in the retail price of conventional fuel f in month m in year t
$perc\_refine_{f,m,t}$	Percentage of refinery cost in the retail price of conventional fuel f in month m in year t

2.8.4 Carbon abatement costs

We collect carbon abatement costs from the above studies. For studies that estimated GHG emissions but did not give abatement costs (2030 MTG-gasoline in Soler et al. [9], 2030 FT-diesel using Germany grid electricity in Hombach et al. [11], and Kannangara et al. [62]), the GHG emissions of conventional fossil fuels (gasoline: 91 g CO_2-eq/MJ; diesel: 92 g CO_2-eq/MJ) from GREET 2022 [8] and their production costs estimated above are used to estimate the carbon abatement cost, shown as formula (10).

$$abate\_cost_{efuel} = \frac{prod\_cost_{efuel} - prod\_cost_f}{ghg_f - ghg_{efuel}} \quad (10)$$

$$f = gasoline,diesel$$

$abate\_cost_{efuel}$	Carbon abatement cost of e-fuels
$prod\_cost_{efuel}$	Production cost of e-fuels (USD2022/MJ)
$prod\_cost_f$	Production cost of conventional fuel f (USD2022/MJ)
ghg_f	GHG emissions of e-fuels (t CO_2-eq/MJ)
ghg_{efuel}	GHG emissions of conventional fuel f (t CO_2-eq/MJ)

To illustrate the relationship between carbon abatement costs of e-fuels and the emission factors of electricity used in e-fuel production, we further collect the latter from the above studies. For the three studies that did not specify the electricity emission factors, we estimate them as follows. Several scenarios in Hombach et al. [11] used wind electricity for water electrolysis and the Germany grid mix electricity for DAC and syngas compression. The weighted average of the electricity emission factor based on the amount of electricity used in each step is adopted. Ordóñez et al. [39] did not specify the emission factor of offshore wind

electricity but provided the amount of offshore wind electricity used for e-fuel production and the GHG emissions when the environmental impacts of wind electricity are included and excluded from the calculation. Therefore, the emission factor of wind electricity is back-calculated to be around 15 g CO_2-eq/kWh. Ueckerdt et al. [63] did not specify the emission factor of renewable electricity during 2020-2025, and the emission factor of renewable electricity (26 g CO_2-eq/kWh) in 2030 is assumed.

2.8.5 Social cost of carbon

Social costs of CO_2 emitted from 2020 to 2050 are collected from the draft report from the U.S. Environmental Protection Agency (EPA) [72]. The values are then adjusted to USD2022 using CPI. The resulting social costs of carbon are shown in **Table S22**.

Table S22 Social costs of carbon emitted from 2020 to 2050 (Source: [72]**)**

Emission year	Discount rate [1]	Social costs of carbon (USD2022/t)
2020	2.50%	136
2020	2.00%	215
2020	1.50%	384
2030	2.50%	158
2030	2.00%	260
2030	1.50%	430
2040	2.50%	192
2040	2.00%	305
2040	1.50%	486
2050	2.50%	226
2050	2.00%	350
2050	1.50%	543

[1] [72] used dynamic discount rates where near-term Ramsey discount rates are 1.5%, 2.0%, and 2.5%.

3. Additional Results

3.1 Comparing fuel-level GHG emissions with other studies

Table S23 compares the fuel-level GHG emissions of e-gasoline in this study with other studies using similar pathways, technologies, and energy sources.

Table S23 Comparison of fuel-level GHG emissions with other studies with similar e-fuel production scenarios

#	Scenario [1]	Fuel-level GHG emissions (g CO_2-eq/MJ) [2,3]		Comparison [3]
		This study	Other studies	
1	FT-ELE-DAC + GRID + NG	AEL: 385	AEL:441 [11] PEM: 608 [8]	• Hombach et al. [11]: This fuel-level emission result corresponds to the scenario where e-gasoline was produced from DAC CO_2 (heat from natural gas) and the 2015 Germany grid, which had an emission factor of 648 g CO_2-eq/kWh. This emission factor is higher than the 2022 U.S. grid (438 g CO_2-eq/kWh), which might contribute to the higher number than this study. • GREET 2022 [8]: This fuel-level GHG emission result corresponds to the scenario where e-gasoline was produced from U.S. grid mix electricity (467 g CO_2-eq/kWh) and CO_2 captured using the low-temperature absorption-based DAC approach under current status powered by natural gas. The higher value than this study might be explained by the higher H_2 and CO_2 demand from RWGS.
2	FT-ELE-DAC + PV + NG	AEL: 124	PEM: 187 [8]	• GREET 2022 [8]: This fuel-level GHG emission result corresponds to the scenario where e-gasoline was produced from solar PV electricity (39.2 g CO_2-eq/kWh) and CO_2 captured using the low-temperature absorption-based DAC approach under current status powered by natural gas. The higher value than this study might be explained by the higher H_2 and CO_2 demand from RWGS.
3	FT-ELE-DAC + WIND + NG	AEL: 105	AEL: 48 [11] PEM: 162 [8]	• Hombach et al. [11]: This fuel-level emission result corresponds to the scenario where e-gasoline was produced from DAC CO_2 (heat from natural gas) and wind electricity (0.174 g CO_2-eq/kWh). The emission factor for wind electricity is lower than the emission factor adopted in this study (10.4 g CO_2-eq/kWh), which might contribute to the lower number than this study. • GREET 2022 [8]: This fuel-level GHG emission result corresponds to the scenario where e-gasoline was produced from wind electricity (10.4 g CO_2-eq/kWh) and CO_2

				captured using the low-temperature absorption-based DAC approach under current status powered by natural gas. The higher value than this study might be explained by the higher H_2 and CO_2 demand from RWGS.
4	FT-ELE-DAC + PV + ST	AEL: 26 PEM: 25	AEL: 22.1 [9]; AEL: 30 [12] PEM: 15 [73]; PEM: 49 [8] Unspecified: 24-32 [63]	• Soler et al. [9]: This fuel-level GHG emission result corresponds to the scenario where the heat for DAC was from electric heaters or heat integration and e-gasoline was produced from the Germany solar PV electricity, which had an emission factor of 31.1 g CO_2-eq/kWh. This emission factor is slightly lower than the emission factor of solar PV adopted in this study (39.2 g CO_2-eq/kWh), which might contribute to the lower number than this study. • Giesen et al. [12]: This fuel-level GHG emission result corresponds to the scenario where CO_2 was captured using the moisture swing process which does not need heat. The electricity used for this scenario was solar PV with an unspecified emission factor. • Isaacs et al. [73]: This fuel-level emission result corresponds to the scenario where e-gasoline was produced from solar PV electricity (26 g CO_2-eq/kWh for the utility scale) and CO_2 captured from DAC without heat input. The electricity emission factor is lower than the emission factors of solar PV electricity adopted in this study (39.2 g CO_2-eq/kWh), which might contribute to the lower number than this study. • GREET 2022 [8]: This fuel-level GHG emission result corresponds to the scenario where e-gasoline was produced from solar PV (39.2 g CO_2-eq/kWh) and CO_2 captured using the low-temperature absorption-based DAC approach under current status powered by waste heat. The higher value than this study might be explained by the higher H_2 and CO_2 demand from RWGS. • Ueckerdt et al. [63]: These fuel-level GHG emission results correspond to the scenarios where AEL or PEM was the electrolysis technology, FT or MTG was the chemical synthesis, the electricity used for e-gasoline production was renewable, and DAC was powered by waste heat. The emission factors of renewable electricity were projected to be 26 g CO_2-eq/kWh in 2030 and 16 g CO_2-eq/kWh in 2050. These emission factors are lower than the emission factors of solar PV electricity adopted in this study (39.2 g CO_2-eq/kWh).
5	FT-ELE-DAC + WIND + ST	AEL: 7 PEM: 7	AEL: 1.28 [11]; AEL: 5.6 [9]; AEL: 12 [74] PEM: 1.3 [75];	• Hombach et al. [11]: This fuel-level emission result corresponds to the scenario where e-gasoline was produced from DAC CO_2 (heated by solar thermal energy) and wind electricity (0.174 g CO_2-eq/kWh). The emission factor for wind electricity is lower than the emission factor adopted in this study (10.4 g CO_2-eq/kWh), which might

			PEM: 2 [73]; PEM: 24 [8] Unspecified: 24-32 [63]	contribute to the lower number than this study. • Soler et al. [9]: This fuel-level GHG emission result corresponds to the scenario where the heat for DAC was from electric heaters or heat integration and e-gasoline was produced from the Norway wind electricity, which had an emission factor of 6.6 g CO_2-eq/kWh. This emission factor is lower than the emission factor of wind power adopted in this study (10.4 g CO_2-eq/kWh), which might contribute to the lower number than this study. • Liu et al. [74]: This fuel-level GHG emission result corresponds to the scenario where CO_2 was captured using electric calciners and e-gasoline was produced using the grid electricity in British Columbia, Canada, which had an emission factor of 13 g CO_2-eq/kWh. The higher emission factor of electricity (10.4 g CO_2-eq/kWh for wind electricity in this study) and the higher electricity demand for AEL electrolyzer (57 kWh/kg H_2 versus 50 kWh/kg H_2 in this study) might contribute to the higher number than this study. • Zang et al. [75]: This fuel-level GHG emission result corresponds to the scenario where H_2 was produced from low-temperature electrolysis. Embodied emissions related to renewable electricity production and carbon capture were excluded from the system boundary, which might contribute to the lower number than this study. • Isaacs et al. [73]: This fuel-level emission result corresponds to the scenario where e-gasoline was produced from onshore wind electricity (11 g CO_2-eq/kWh for utility scale) and CO_2 captured from DAC without heat input. The electricity emission factor is similar to the emission factor of onshore wind electricity adopted in this study (10.4 g CO_2-eq/kWh). • GREET 2022 [8]: This fuel-level GHG emission result corresponds to the scenario where e-gasoline was produced from wind electricity (10.4 g CO_2-eq/kWh) and CO_2 captured using the low-temperature absorption-based DAC approach under current status powered by waste heat. The higher value than this study might be explained by the higher H_2 and CO_2 demand from RWGS. • Ueckerdt et al. [63]: These fuel-level GHG emission results correspond to the scenarios where AEL or PEM was the electrolysis technology, FT or MTG was the chemical synthesis, the electricity used for e-gasoline production was renewable, and DAC was powered by waste heat. The emission factors of renewable electricity were projected to be 26 g CO_2-eq/kWh in 2030 and 16 g CO_2-eq/kWh in 2050. These emission factors are higher than the emission factors of wind power electricity adopted in this study

				(10.4 g CO_2-eq/kWh), which might contribute to higher numbers than this study.
6	FT-ELE-IND + GRID + NA	AEL: 272	PEM: 437 [8]	• GREET 2022 [8]: This fuel-level GHG emission result corresponds to the scenario where e-gasoline was produced from U.S. grid mix electricity (467 g CO_2-eq/kWh) and CO_2 captured from a natural gas combined cycle plant. The higher value than this study might be explained by the higher H_2 and CO_2 demand from RWGS.
7	FT-ELE-IND + PV + NA	AEL: 24	AEL: 12 [9] PEM: 41 [8] Unspecified: 4 [76]	• Soler et al. [9]: This fuel-level GHG emission result corresponds to the scenario where CO_2 was captured from the flue gas from steam methane reforming (SMR) and e-gasoline was produced from the Germany renewable electricity, which had an emission factor of 17.7 g CO_2-eq/kWh. This emission factor is lower than the emission factor of solar PV electricity adopted in this study (39.2 g CO_2-eq/kWh), which might contribute to the lower number than this study. • GREET 2022 [8]: This fuel-level GHG emission result corresponds to the scenario where e-gasoline was produced from solar PV electricity (39.2 g CO_2-eq/kWh) and CO_2 captured from a natural gas combined cycle plant. The higher value than this study might be explained by the higher H_2 and CO_2 demand from RWGS. • Kelly et al. [76]: This fuel-level GHG emission result corresponds to the scenario where e-gasoline was produced from renewable electricity. The electrolysis technology was not specified but it would not affect the results as electricity generation from wind and solar PV was assumed to have no emission. CO_2 was captured from high-purity CO_2 sources and thus no energy consumption was related to carbon capture. These assumptions might contribute to the lower number than this study.
8	FT-ELE-IND + WIND + NA	AEL: 6	AEL: 12 [9] PEM: 16 [8] Unspecified: 4 [76]	• Soler et al. [9]: This fuel-level GHG emission result corresponds to the scenario where CO_2 was captured from the flue gas from steam methane reforming (SMR) and e-gasoline was produced from the Germany renewable electricity, which had an emission factor of 17.7 g CO_2-eq/kWh. This emission factor is higher than the emission factor of wind power adopted in this study (10.4 g CO_2-eq/kWh), which might contribute to the higher number than this study. • GREET 2022 [8]: This fuel-level GHG emission result corresponds to the scenario where e-gasoline was produced from wind electricity (10.4 g CO_2-eq/kWh) and CO_2 captured from a natural gas combined cycle plant. The higher value than this study might be explained by the higher H_2 and CO_2 demand from RWGS. • Kelly et al. [76]: This fuel-level GHG emission result corresponds to the scenario where e-gasoline was produced from renewable electricity. The electrolysis technology was not specified but it would not affect the results as electricity generation from wind

				and solar PV was assumed to be no emission. CO_2 was captured from high-purity CO_2 sources and thus no energy consumption was related to carbon capture. These assumptions might contribute to the lower number than this study.
9	FT-COE-DAC + GRID + NG	SOEC: 348	SOEC: 107 [11]	• Hombach et al. [11]: This fuel-level emission result corresponds to the scenario where e-gasoline was produced from the 2030 Germany grid, which was projected to have an emission factor of 374.4 g CO_2-eq/kWh. This emission factor is lower than the 2022 U.S. grid (438 g CO_2-eq/kWh). They also assumed that DAC in 2030 will not require heat. These assumptions might contribute to the lower number than this study.
10	FT-COE-DAC + PV+ NG	SOEC: 121	NA	NA
11	FT-COE-DAC + WIND + NG	SOEC: 104	NA	NA
12	FT-COE-DAC + PV + ST	SOEC: 23	SOEC: 16 [73]	• Isaacs et al. [73]: This fuel-level emission result corresponds to the scenario where e-gasoline was produced from solar PV electricity (26 g CO_2-eq/kWh for utility scale) and CO_2 captured from DAC without heat input. The electricity emission factor is lower than the emission factors of solar PV electricity adopted in this study (39.2 g CO_2-eq/kWh), which might contribute to the lower number than this study.
13	FT-COE-DAC + WIND + ST	SOEC: 6	SOEC: 6 [73]	• Isaacs et al. [73]: This fuel-level emission result corresponds to the scenario where e-gasoline was produced from onshore wind electricity (11 g CO_2-eq/kWh for the utility scale) and CO_2 captured from DAC without heat input. The electricity emission factor is similar to the emission factors of onshore wind electricity adopted in this study (10.4 g CO_2-eq/kWh).
14	FT-COE-IND + GRID + NA	SOEC: 235	NA	NA
15	FT-COE-IND + PV + NA	SOEC: 21	Unspecified: 4 [76]	• Kelly et al. [76]: This fuel-level GHG emission result corresponds to the scenario where e-gasoline was produced from renewable electricity. The electrolysis technology was not specified but it would not affect the results as electricity generation from wind and solar PV was assumed to be no emission. CO_2 was captured from high-purity CO_2 sources and thus no energy consumption was related to carbon capture. These assumptions might contribute to the lower number than this study.
16	FT-COE-IND + WIND + NA	SOEC: 6	SOEC: -45 [39] Unspecified: 4 [76]	• Ordóñez et al. [39]: This fuel-level GHG emission result corresponds to the scenario where CO_2 was captured from the flue gas from coal power plants. The number is negative because the emissions from fuel combustion were not included. If the emissions from fuel combustion in GREET 2022 (73 g CO_2-eq/MJ) were adopted, the

				number would become 28 g CO_2-eq/MJ. The electricity for this scenario is wind electricity with an unspecified emission factor. • Kelly et al. [76]: This fuel-level GHG emission result corresponds to the scenario where e-gasoline was produced from renewable electricity. The electrolysis technology was not specified but it would not affect the results as electricity generation from wind and solar PV was assumed to be no emission. CO_2 was captured from high-purity CO_2 sources and thus no energy consumption was related to carbon capture. These assumptions might contribute to the lower number than this study.
17	MTG-ELE-DAC + GRID + NG	AEL: 338	NA	NA
18	MTG-ELE-DAC + PV + NG	AEL: 106	NA	NA
19	MTG-ELE-DAC + WIND + NG	AEL: 89	NA	NA
20	MTG-ELE-DAC + PV + ST	AEL: 23	Unspecified: 24-32 [63]	• Ueckerdt et al. [63]: These fuel-level GHG emission results correspond to the scenarios where AEL or PEM was the electrolysis technology, FT or MTG was the chemical synthesis, the electricity used for e-gasoline production was renewable, and DAC was powered by waste heat. The emission factors of renewable electricity were projected to be 26 g CO_2-eq/kWh in 2030 and 16 g CO_2-eq/kWh in 2050. These emission factors are lower than the emission factors of solar PV electricity adopted in this study (39.2 g CO_2-eq/kWh).
21	MTG-ELE-DAC + WIND + ST	AEL: 6	AEL: 5.4 [9] Unspecified: 24-32 [63]	• Soler et al. [9]: This fuel-level GHG emission result corresponds to the scenario where the heat for DAC was from electric heaters or heat integration and e-gasoline was produced from the Norway wind electricity, which had an emission factor of 6.6 g CO_2-eq/kWh. This emission factor is lower than the emission factor of wind power adopted in this study (10.4 g CO_2-eq/kWh), which might contribute to the lower number than this study. • Ueckerdt et al. [63]: These fuel-level GHG emission results correspond to the scenarios where AEL or PEM was the electrolysis technology, FT or MTG was the chemical synthesis, the electricity used for e-gasoline production was renewable, and DAC was powered by waste heat. The emission factors of renewable electricity were projected to be 26 g CO_2-eq/kWh in 2030 and 16 g CO_2-eq/kWh in 2050. These emission factors are higher than the emission factors of wind power electricity adopted in this study (10.4 g CO_2-eq/kWh).

22	MTG-ELE-IND + GRID + NA	AEL: 242	NA	NA
23	MTG-ELE-IND + PV + NA	AEL: 22	AEL: 11 [9]	• Soler et al. [9]: This fuel-level GHG emission result corresponds to the scenario where CO_2 was captured from the flue gas from steam methane reforming (SMR) and e-gasoline was produced from the Germany renewable electricity, which had an emission factor of 17.7 g CO_2-eq/kWh. This emission factor is lower than the emission factor of solar PV power adopted in this study (39.2 g CO_2-eq/kWh), which might contribute to the lower number than this study.
24	MTG-ELE-IND + WIND + NA	AEL: 6	AEL: 11 [9]	• Soler et al. [9]: This fuel-level GHG emission result corresponds to the scenario where CO_2 was captured from the flue gas from steam methane reforming (SMR) and e-gasoline was produced from the Germany renewable electricity, which had an emission factor of 17.7 g CO_2-eq/kWh. This emission factor is higher than the emission factor of wind power adopted in this study (10.4 g CO_2-eq/kWh), which might contribute to the higher number than this study.

[1] Scenarios are named using the following rule: "production pathway" - "CO_2 source" + "electricity source" + "heat source". FT = FT gasoline; MTG = MTG-gasoline; ELE = electrolysis-based production pathway; COE = co-electrolysis-based production pathway; DAC = direct air capture; IND = post-combustion industrial flue gas; GRID = 2022 U.S. grid electricity; PV = solar PV; WIND = onshore wind power; NG = natural gas; ST = solar thermal energy; NA = not applicable.

[2] Electrolysis technologies: AEL, alkaline electrolysis; SOEC, solid oxide electrolyzer cell; PEM, proton exchange membrane. Unspecified = unspecified in the source text which electrolysis technology was applied.

[3] NA = no available data.

3.2 Break-even emission factor of electricity used for e-gasoline production

Table S24 shows the break-even emission factor of electricity between e-gasoline and conventional gasoline.

Table S24 Break-even emission factor of electricity between e-gasoline and conventional gasoline

NO	Scenario [1]	Break-even emission factor of electricity between e-gasoline and conventional gasoline (g CO_2-eq/kWh)	
		Electrolysis or co-electrolysis only	Overall e-gasoline production
1	FT-ELE-DAC + ST	100	139
2	FT-ELE-IND + NA	125	147
3	FT-COE-DAC + ST	121	159
4	FT-COE-IND + NA	151	169
5	MTG-ELE-DAC + ST	116	156
6	MTG-ELE-IND + NA	141	164

[1] Scenarios are named using the following rule: "production pathway" - "CO_2 source" + "electricity source" + "heat source". FT = FT gasoline; MTG = MTG-gasoline; ELE = electrolysis-based production pathway; COE = co-electrolysis-based production pathway; DAC = direct air capture; IND = post-combustion industrial flue gas; GRID = 2022 U.S. grid electricity; PV = solar PV; WIND = onshore wind power; NG = natural gas; ST = solar thermal energy; NA = not applicable. Scenarios with natural gas as the heat source are removed as the resulting e-gasoline would have higher GHG emissions than conventional gasoline.

3.3 Sensitivity analysis of data sources on fuel-level results

Figure S3 illustrates the variations in fuel-level GHG emissions of e-gasoline when different data sources on mass and energy balance are used.

The default data sources generate generally higher estimates than other sources due to the higher energy consumption in carbon capture from GREET 2022 [8]. The data from Ordóñez et al. [39] generate higher fuel-level GHG emissions from e-gasoline produced from co-electrolysis-based production pathways as they assumed lower power-to-fuel efficiency of SOEC. The demands for H_2 and CO_2 in RWGS and FT process in GREET 2022 are substantially higher than other data sources [8], resulting in more than 50% higher fuel-level GHG emissions in FT-gasoline produced from non-renewable energy sources than this study (430-630 g CO_2-eq/MJ when using GREET 2022 data versus 270-390 g CO_2-eq/MJ in this study). Due to the higher heat demand by DAC in this study, the selection of data sources would impact the conclusion regarding whether a low-carbon heat source for DAC is a necessary condition to render e-gasoline less GHG intensive than conventional gasoline. Our adoption of heat demand for the current low-temperature DAC technology in GREET 2022 [8] results in higher fuel-level GHG emissions of e-gasoline than that of conventional gasoline as long as it is heated by natural

gas. However, this is not the case when data sources with lower heat demand by DAC are employed. Switching to data sources using less heat by DAC would decrease the fuel-level GHG emissions from e-gasoline to levels that are lower than conventional gasoline even if natural gas is the heat source for DAC, when renewable electricity is used. Therefore, using these data sources would expand the choices of e-gasoline production scenarios that have mitigation potential in the U.S. LDV fleet and reduce the demand for e-gasoline to bridge mitigation gaps.

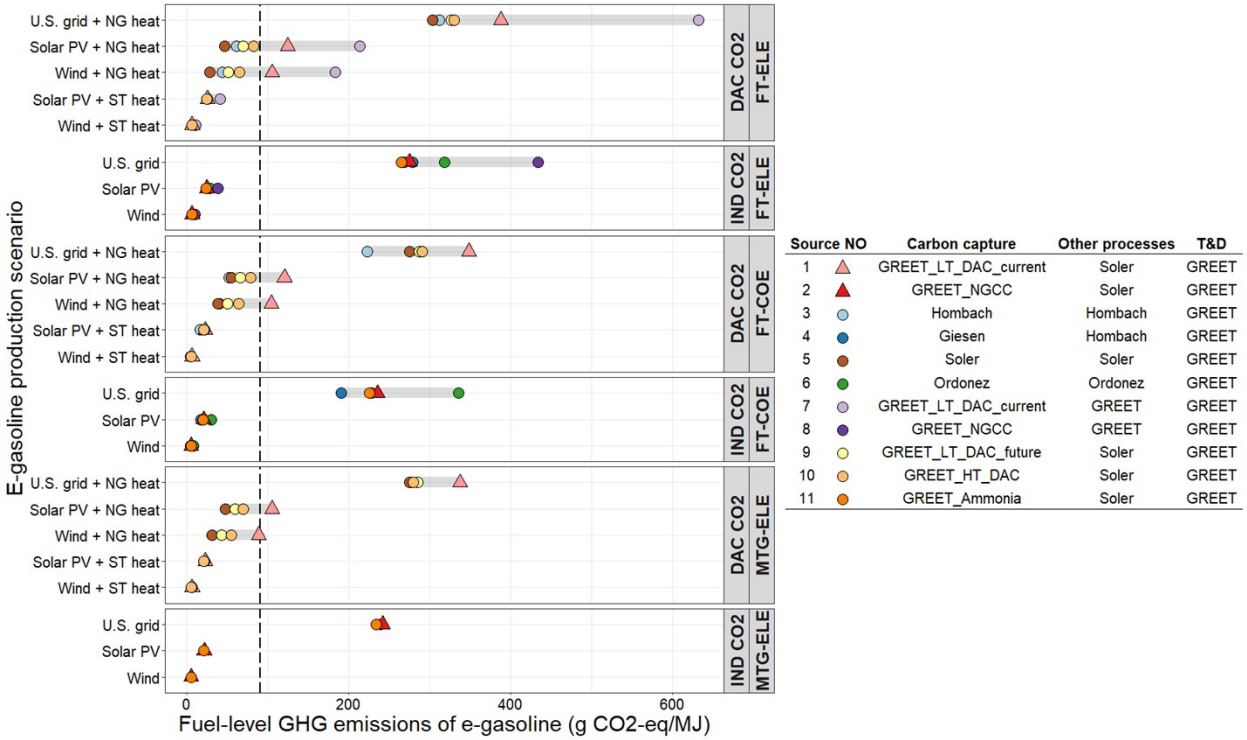

Figure S3 Comparison of fuel-level GHG emissions from e-gasoline using various data sources on mass and energy balance. For energy sources on the y-axis, the first term is the electricity source for all stages of e-gasoline production, and the second term is the heat source for direct air capture (DAC) as industrial carbon capture (IND) does not require external heat. Emissions of e-gasoline include emissions from carbon capture, water electrolysis or co-electrolysis, syngas production, methanol synthesis, Fischer-Tropsch (FT) process, and methanol-to-gasoline (MTG) process. No direct emissions are assumed for fuel combustion for e-gasoline. Triangles represent the default data sources used in the study and circles represent alternate data sources. A detailed description of data sources is in SI Section 2.1. Abbreviations: ELE: electrolysis; COE: co-electrolysis; NG: natural gas; ST: solar thermal.

3.4 Contribution analysis of vehicle-level GHG emissions

Figure S4 shows the vehicle-level GHG emissions from BEVs, PHEVs, HEVs, and ICEVs-G using conventional gasoline or e-gasoline for both cars and light trucks. The e-gasoline fuel production pathway used here is the FT-gasoline produced from the electrolysis-based production pathway where AEL is used for hydrogen production and DAC heated by solar thermal heat is used for carbon capture. Vehicles of model year 2022 with 15 years of lifetime

are used. The lifetime travel distances for a car and a light truck are assumed to be 278,660 km and 295,094 km, respectively. We assume that the embodied emissions from producing a BEV are higher than an ICEV-G (38 g CO_2-eq/vkt for a BEV300 car, 19 g CO_2-eq/vkt for an ICEV-G car).

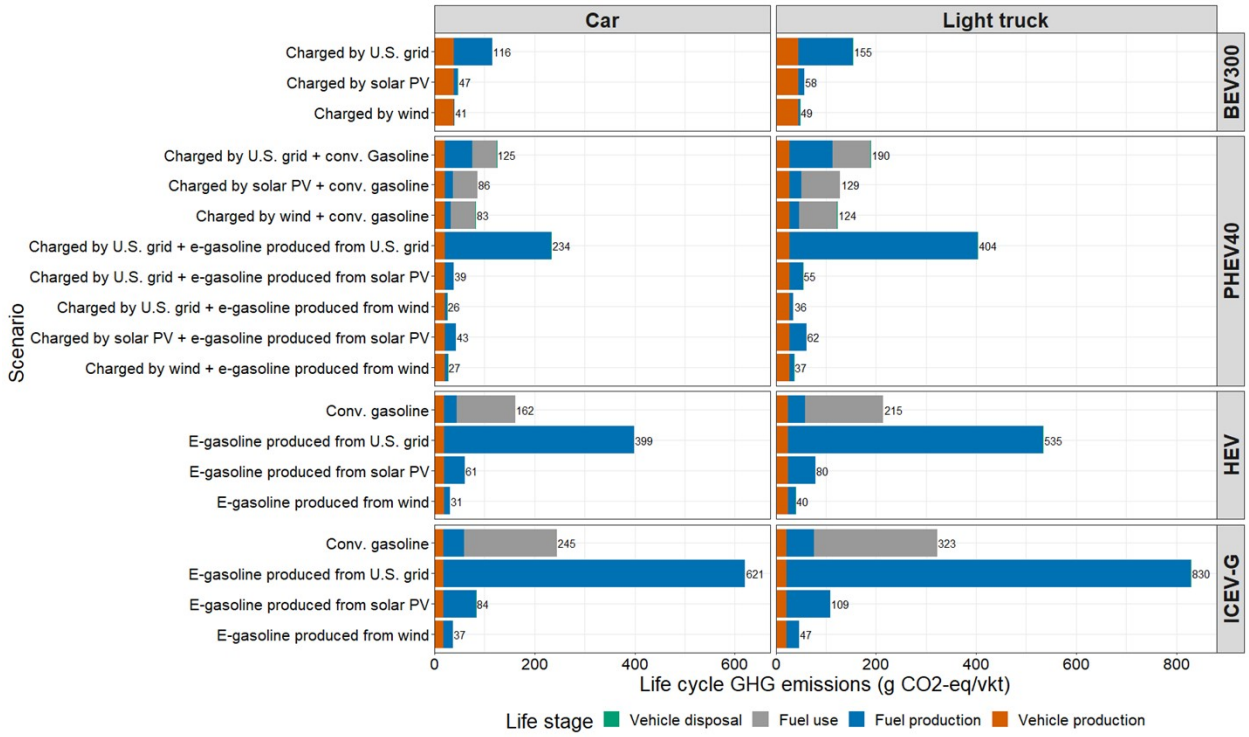

Figure S4 Vehicle-level life cycle GHG emissions from BEV300, PHEV40, HEV, and ICEV-G for cars and light trucks under scenarios (Unit: kg CO_2-eq per vehicle km traveled). For battery electric vehicles (BEVs) and plug-in hybrid electric vehicles (PHEVs), the charging electricity source can be the 2022 U.S. grid electricity (438 g CO_2-eq/kWh), solar PV electricity (39.2 g CO_2-eq/kWh), or wind electricity (10.4 g CO_2-eq/kWh). For PHEVs, hybrid electric vehicles (HEVs), and internal combustion engine vehicles using gasoline (ICEVs-G), drop-in fuel can be conventional gasoline or e-gasoline. The e-gasoline fuel production pathway used here is the Fischer-Tropsch gasoline produced from the electrolysis-based production pathway where alkaline electrolysis is used for hydrogen production, and direct air capture heated by solar thermal heat is used for carbon capture. No emissions are assumed for fuel combustion for e-gasoline as carbon is captured from the atmosphere.

3.5 Well-to-wheel efficiency comparison

Figure S5 shows the well-to-wheel efficiencies of BEVs, ICEVs-G using e-gasoline, HEVs using e-gasoline, and FCEVs. The well-to-wheel efficiencies are substantially lower for ICEVs-G and HEVs using e-gasoline, mainly due to the low tank-to-wheel efficiencies and the low efficiencies in chemical reactions related to e-gasoline production.

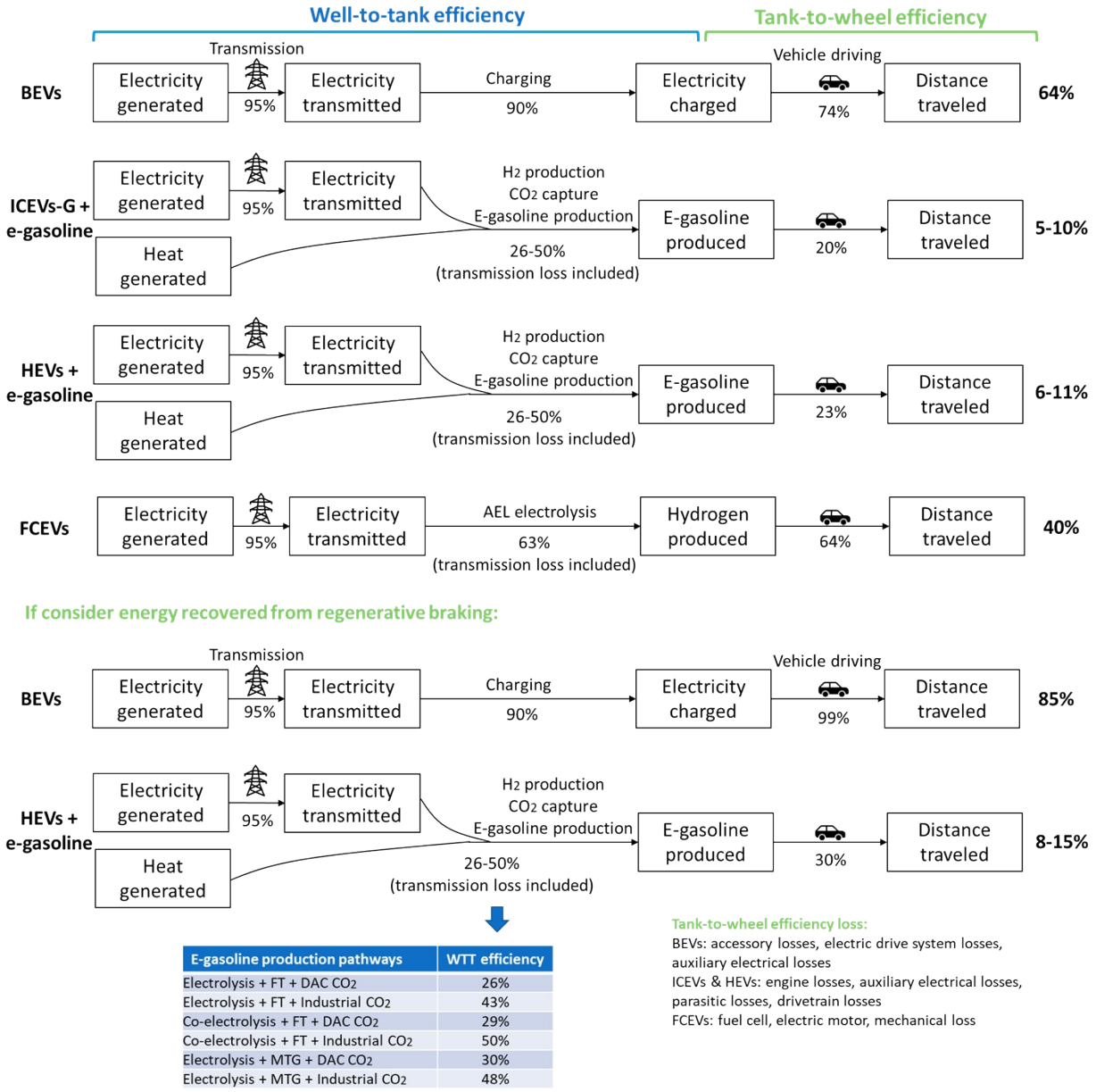

E-gasoline production pathways	WTT efficiency
Electrolysis + FT + DAC CO_2	26%
Electrolysis + FT + Industrial CO_2	43%
Co-electrolysis + FT + DAC CO_2	29%
Co-electrolysis + FT + Industrial CO_2	50%
Electrolysis + MTG + DAC CO_2	30%
Electrolysis + MTG + Industrial CO_2	48%

Figure S5 Well-to-wheel efficiency of BEVs, ICEVs-G using e-gasoline, HEVs using e-gasoline, and FCEVs. E-gasoline refers to Fischer-Tropsch (FT) gasoline and methanol-to-gasoline (MTG) gasoline. Electrolysis is represented by alkaline electrolysis. The efficiency of water electrolysis is based on the lower heating value (LHV) of hydrogen (119.96 MJ/kg). The efficiency of e-gasoline production is based on the LHV of e-gasoline (30.9 MJ/L). The tank-to-wheel efficiencies for battery electric vehicles (BEVs) and hybrid electric vehicles (HEVs) in the upper panel do not consider energy recovered from regenerative braking while those in the lower panel consider.
Abbreviations: ICEVs-G: internal combustion engine vehicle using gasoline; FCEVs: fuel cell electric vehicles; DAC: direct air capture; WTT: well-to-tank.

3.6 Fleet composition

Figure S6 shows the vehicle sales and stock by technology during 2020-2050 under the business-as-usual BEV deployment scenario (BAU BEV) and high BEV deployment scenario (high BEV).

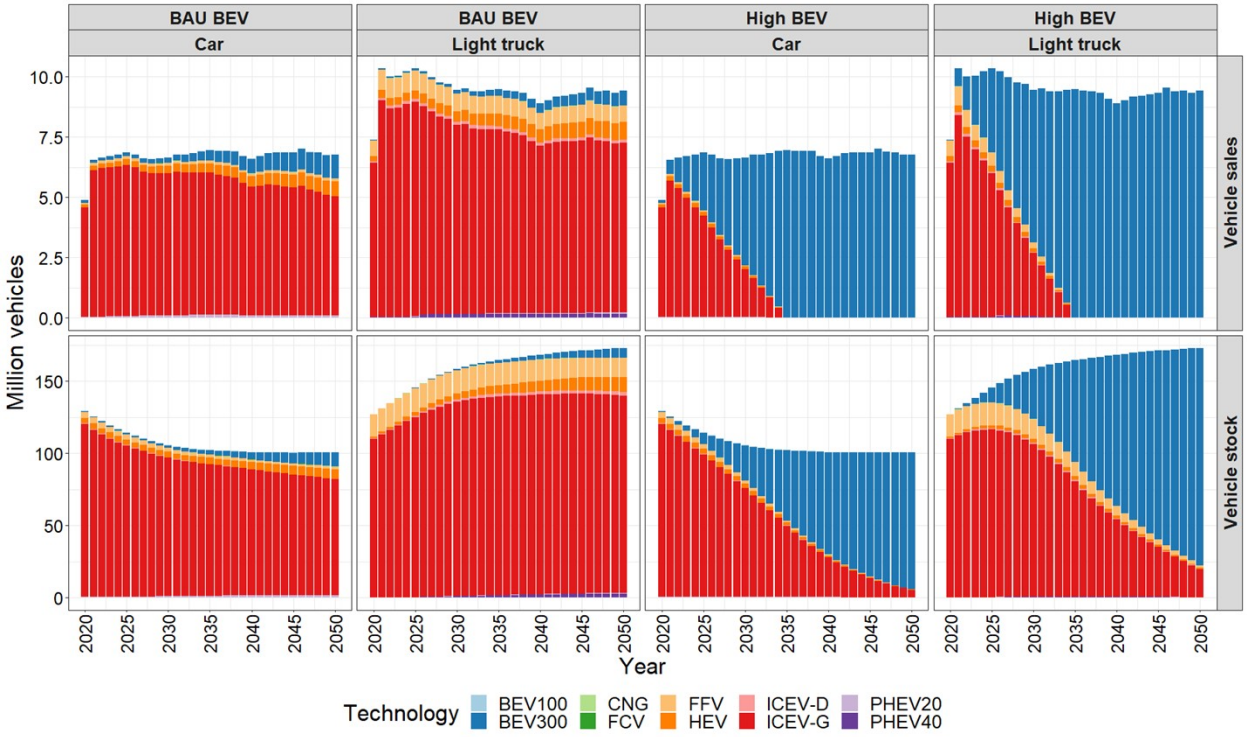

Figure S6 LDV sales and stock by vehicle technology under the BAU BEV and high BEV scenarios during 2020-2050.

Abbreviations: BAU: business-as-usual; BEV: battery electric vehicle; CNG: compressed natural gas; FCV: fuel cell vehicle; FFV: flexible fuel vehicle; HEV: hybrid electric vehicle; ICEV-D: internal combustion engine vehicle using diesel; ICEV-G: internal combustion engine vehicle using gasoline; PHEV: plug-in hybrid electric vehicle.

3.7 Demand for e-gasoline under other e-gasoline production scenarios

Figure S7 shows the annual demand for e-gasoline to meet 1.5 and 2 °C climate targets under various BEV deployment and e-gasoline production scenarios.

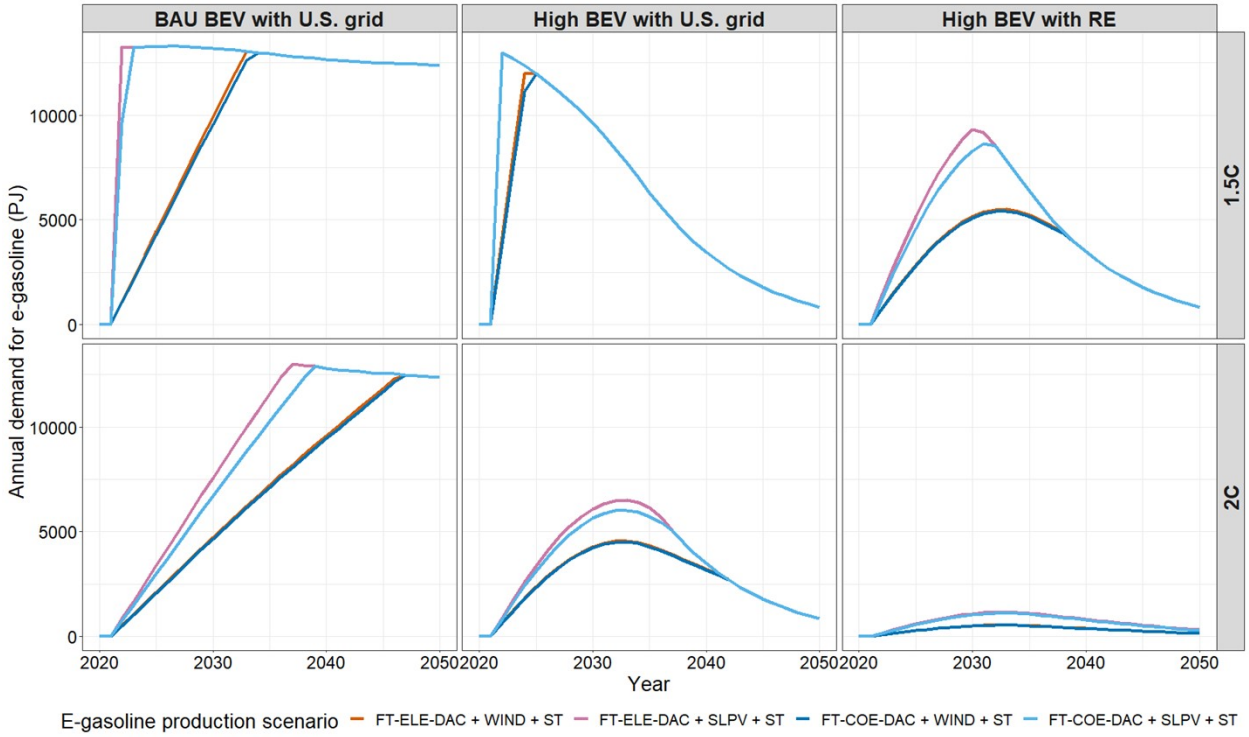

Figure S7 Annual demand for e-gasoline from 2020 to 2050 under various e-gasoline production scenarios.
Abbreviations: BAU: business-as-usual; BEV: battery electric vehicle; RE: renewable electricity; FT: Fischer-Tropsch; ELE: electrolysis; COE: co-electrolysis; DAC: direct air capture; WIND: wind electricity; SLPV: solar PV electricity.

3.8 Demand for feedstock and renewable electricity

3.8.1 Demand for feedstock and renewable electricity under various e-gasoline production scenarios

Table S25, Table S26, **Table S27**, and **Table S28** present the peak annual demand for captured carbon, hydrogen, syngas, and renewable electricity for e-gasoline production under various e-gasoline production scenarios.

Table S25 Peak annual demand for e-gasoline feedstock and energy carriers for U.S. LDV fleet to meet climate targets with mature production pathway best-case for e-gasoline production [1]

Feedstock or energy carrier	Unit	Climate target	Peak annual demand			Current and projected production levels
			BAU BEV with U.S. grid	High BEV with U.S. grid	High BEV with RE	
Captured CO_2	Gt	1.5 °C	1.1	1.1	0.48	U.S. (2023): 0.022 [77] Global (2023): 0.05 [77]
		2 °C	1.1	0.4	0.047	

						Global (2030): 0.44 [77]
Electrolytic H_2	Mt	1.5 °C	150	140	64	U.S. (2020): 0.1 [78] Global (2020): 1.4 [78] Global (2030): 37 [79]
		2 °C	140	53	6.2	
Renewable electricity	TWh	1.5 °C	8500	7800	3600	U.S. (2022): 913 [80] U.S. (2050): 2060 [10] Global (2021): 7900 [81]
		2 °C	8200	3000	350	

[1] Mature production pathway best-case: Fischer-Tropsch gasoline produced from electrolysis-based pathway, direct air capture CO_2, wind electricity, and solar thermal heat.

Table S26 Peak annual demand for e-gasoline feedstock and energy carriers for U.S. LDV fleet to meet climate targets with mature production pathway mid-case for e-gasoline production [1]

Feedstock or energy carrier	Unit	Climate targets	Peak annual demand			Current and projected production levels
			BAU BEV with U.S. grid	High BEV with U.S. grid	High BEV with RE	
Captured CO_2	Gt	1.5 °C	1.2	1.1	0.82	U.S. (2023): 0.022 [77] Global (2023): 0.05 [77] Global (2030): 0.44 [77]
		2 °C	1.1	0.57	0.1	
Electrolytic H_2	Mt	1.5 °C	150	150	110	U.S. (2020): 0.1 [78] Global (2020): 1.4 [78] Global (2030): 37 [79]
		2 °C	150	75	13	
Renewable electricity	TWh	1.5 °C	8700	8500	6100	U.S. (2022): 913 [80] U.S. (2050): 2060 [10] Global (2021): 7900 [81]
		2 °C	8500	4200	760	

[1] Mature production pathway mid-case: Fischer-Tropsch gasoline produced from electrolysis-based pathway, direct air capture CO_2, solar photovoltaic electricity, and solar thermal heat.

Table S27 Peak annual demand for e-gasoline feedstock and energy carriers for U.S. LDV fleet to meet climate targets with advanced production pathway best-case for e-gasoline production [1]

Feedstock or energy carrier	Unit	Climate targets	Peak annual demand			Current and projected production levels
			BAU BEV with U.S. grid	High BEV with U.S. grid	High BEV with RE	
Captured CO_2	Gt	1.5 °C	1.1	1.1	0.48	U.S. (2023): 0.022 [77] Global (2023): 0.05 [77] Global (2030): 0.44 [77]
		2 °C	1.1	0.4	0.046	
Syngas (Co-electrolysis)	Mt	1.5 °C	830	760	340	No available data
		2 °C	790	290	34	
Renewable electricity	TWh	1.5 °C	7400	6800	3100	U.S. (2022): 913 [80] U.S. (2050): 2060 [10] Global (2021): 7900 [81]
		2 °C	7100	2600	300	

[1] Advanced production pathway best-case: Fischer-Tropsch gasoline produced from co-electrolysis-based pathway, direct air capture CO_2, wind electricity, and solar thermal heat.

Table S28 Peak annual demand for e-gasoline feedstock and energy carriers for U.S. LDV fleet to meet climate targets with advanced production pathway mid-case for e-gasoline production [1]

Feedstock or energy carrier	Unit	Climate targets	Peak annual demand			Current and projected production levels
			BAU BEV with U.S. grid	High BEV with U.S. grid	High BEV with RE	
Captured CO_2	Gt	1.5 °C	1.2	1.1	0.76	U.S. (2023): 0.022 [77] Global (2023): 0.05 [77] Global (2030): 0.44 [77]
		2 °C	1.1	0.53	0.097	
Syngas (Co-electrolysis)	Mt	1.5 °C	840	830	550	No available data
		2 °C	820	380	70	
Renewable	TWh	1.5 °C	7600	7400	4900	U.S. (2022): 913 [80] U.S. (2050): 2060

						[10] Global (2021): 7900 [81]

[1] Advanced production pathway mid-case: Fischer-Tropsch gasoline produced from co-electrolysis-based pathway, direct air capture CO_2, solar photovoltaic electricity, and solar thermal heat.

3.8.2 Comparing demand for feedstock and renewable electricity in baseline scenario with other studies

Figure S8 and **Figure S9** show the annual demand for captured CO_2, electricity, and H_2 in the U.S. LDV fleet to meet the 1.5 °C and 2 °C climate targets under different BEV deployment scenarios. The e-gasoline fuel production pathway used here is the FT-gasoline produced from the electrolysis-based production pathway where AEL is used for hydrogen production, wind electricity is used for the whole e-gasoline production chain, and DAC is heated by solar thermal energy.

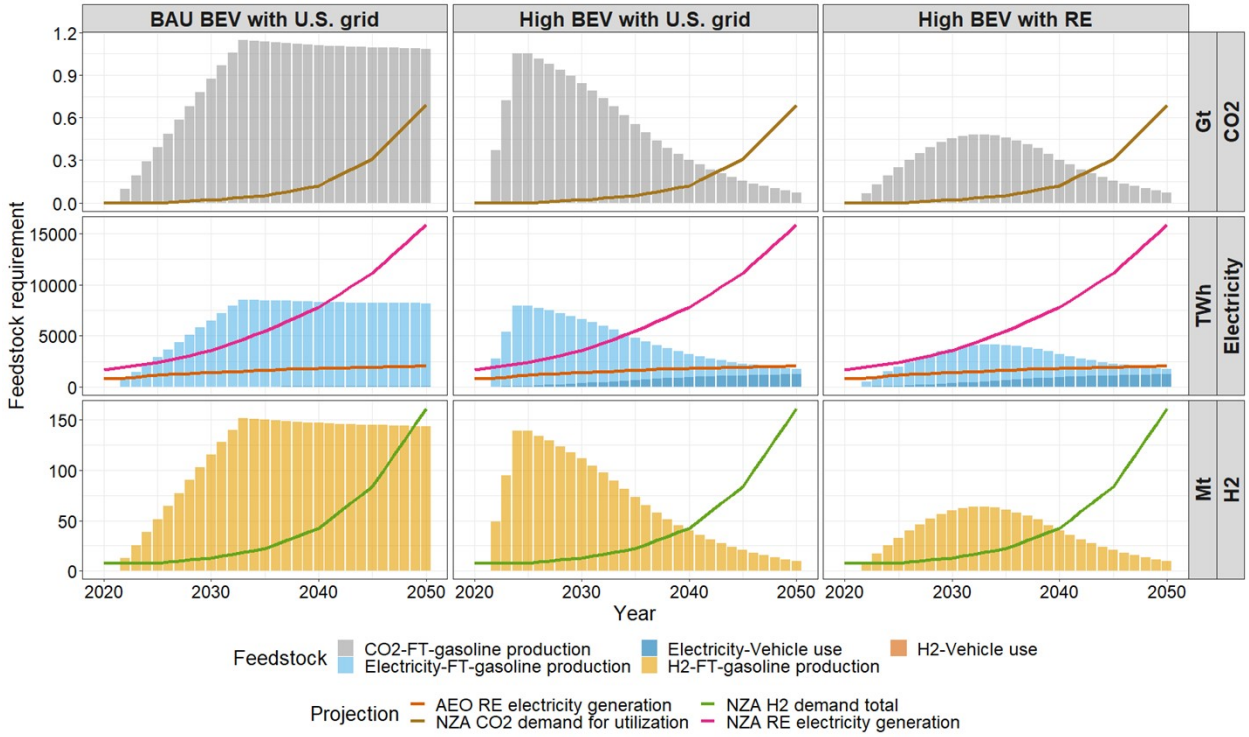

Figure S8 2020-2050 annual demand for CO_2, electricity, and H_2 for U.S. LDV fleet under various scenarios to meet the 1.5 ˚C climate target. "Electricity-Vehicle use" includes electricity used for charging electric vehicles but excludes electricity used to produce H_2 for direct use in hydrogen fuel cell electric vehicles (whose numbers are projected to be low). For comparison, projection data are collected from the Annual Energy Outlook (AEO) 2022 reference case [10], [82], and the Princeton Net Zero America (NZA) E+RE+ scenario [6]. The e-gasoline fuel production pathway used here is the Fischer-Tropsch gasoline produced from the electrolysis-based production pathway where alkaline electrolysis is

used for hydrogen production, wind electricity is used for the whole e-gasoline production chain, and direct air capture is heated by solar thermal energy. Abbreviation: RE: renewable electricity.

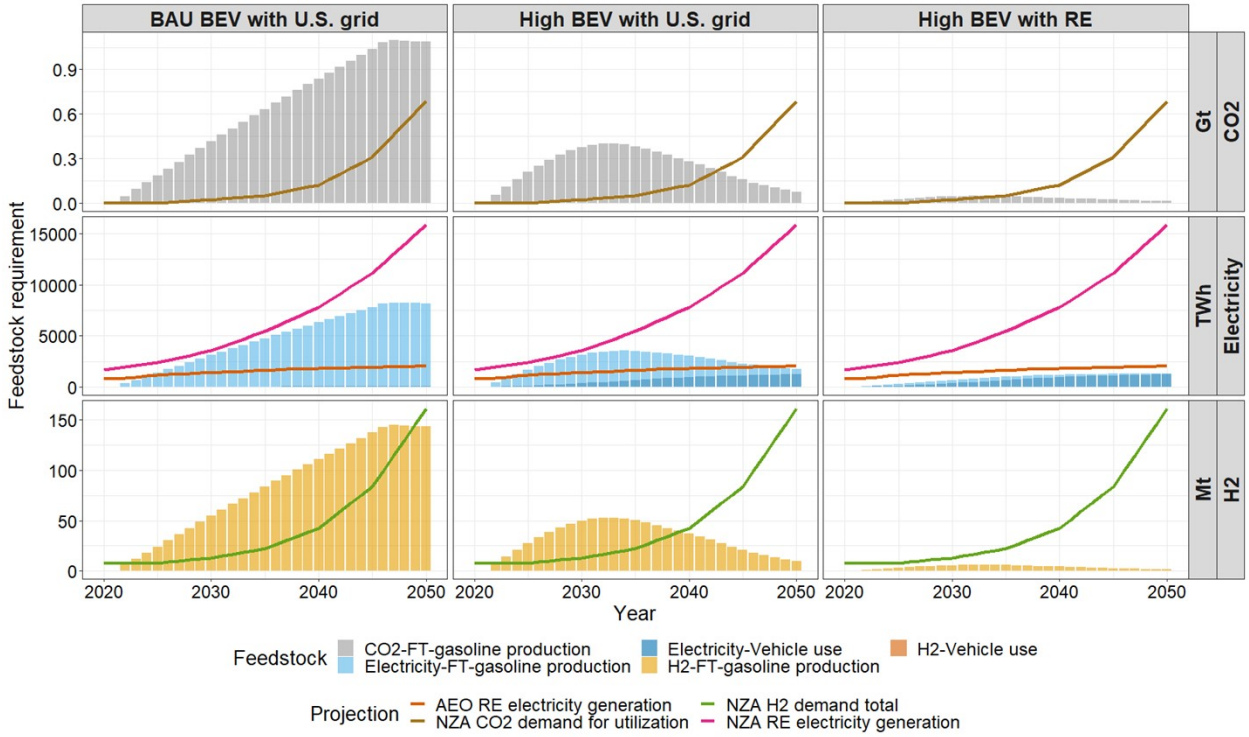

Figure S9 2020-2050 annual demand for CO_2, electricity, and H_2 for U.S. LDV fleet under various scenarios to meet the 2 ˚C climate target. "Electricity-Vehicle use" includes electricity used for charging electric vehicles but excludes electricity used to produce H_2 for direct use in hydrogen fuel cell electric vehicles (whose numbers are projected to be low). For comparison, projection data are collected from the AEO reference case [10], [82], and the Princeton NZA E+RE+ scenario [6]. The e-gasoline fuel production pathway used here is the Fischer-Tropsch gasoline produced from the electrolysis-based production pathway where alkaline electrolysis is used for hydrogen production, wind electricity is used for the whole e-gasoline production chain, and direct air capture is heated by solar thermal energy. Abbreviation: RE: renewable electricity.

3.9 Demand for critical materials from water electrolyzers and RE generation

3.9.1 Cumulative demand for critical materials from water electrolyzers

Figure S10 and **Figure S11** present the cumulative demand for critical materials from water electrolyzers to meet the 2 °C climate target with e-gasoline produced from wind electricity under the BAU BEV with U.S. grid and high BEV with RE scenarios, respectively. **Figure S12** presents the highest cumulative demand for critical materials from water electrolyzers, when FT-gasoline is produced from solar PV electricity under the BAU BEV with U.S. grid scenario to meet the 1.5 °C climate target. Other scenarios are similar to the presented ones (especially within the same BEV deployment scenario), and so results are not shown.

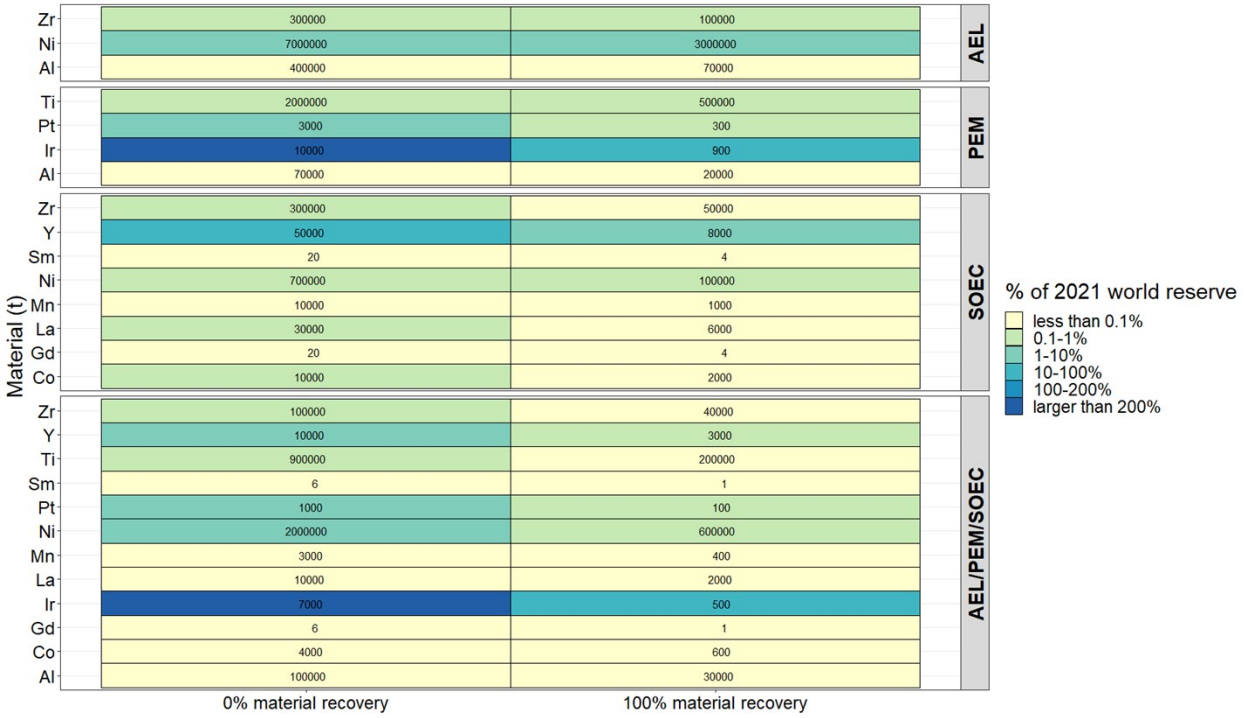

Figure S10 Cumulative demand from 2020 to 2050 for critical materials from water electrolyzers with 0% and 100% material recovery under the BAU BEV with U.S. grid scenario to meet the 2 ˚C climate target with e-gasoline produced from wind electricity. These fleet-level results correspond with Fischer-Tropsch gasoline produced from direct air capture CO_2 and powered by wind electricity and solar thermal heat. The first three panels represent scenarios with 100% of a certain electrolyzer technology, and the last panel represents a scenario with a 20% share of alkaline electrolysis (AEL), 50% of proton exchange membrane (PEM), and 30% of solid oxide electrolyzer cell (SOEC). We include material use for water electrolyzers only for e-gasoline production but not for hydrogen production for fuel cell vehicles. Abbreviations: Al: aluminum; Co: cobalt; Gd: gadolinium; Ir: iridium; La: lanthanum; Mn: manganese; Ni: nickel; Pt: platinum; Sm: Samarium; Ti: titanium; Y: yttrium; Zr: zirconium.

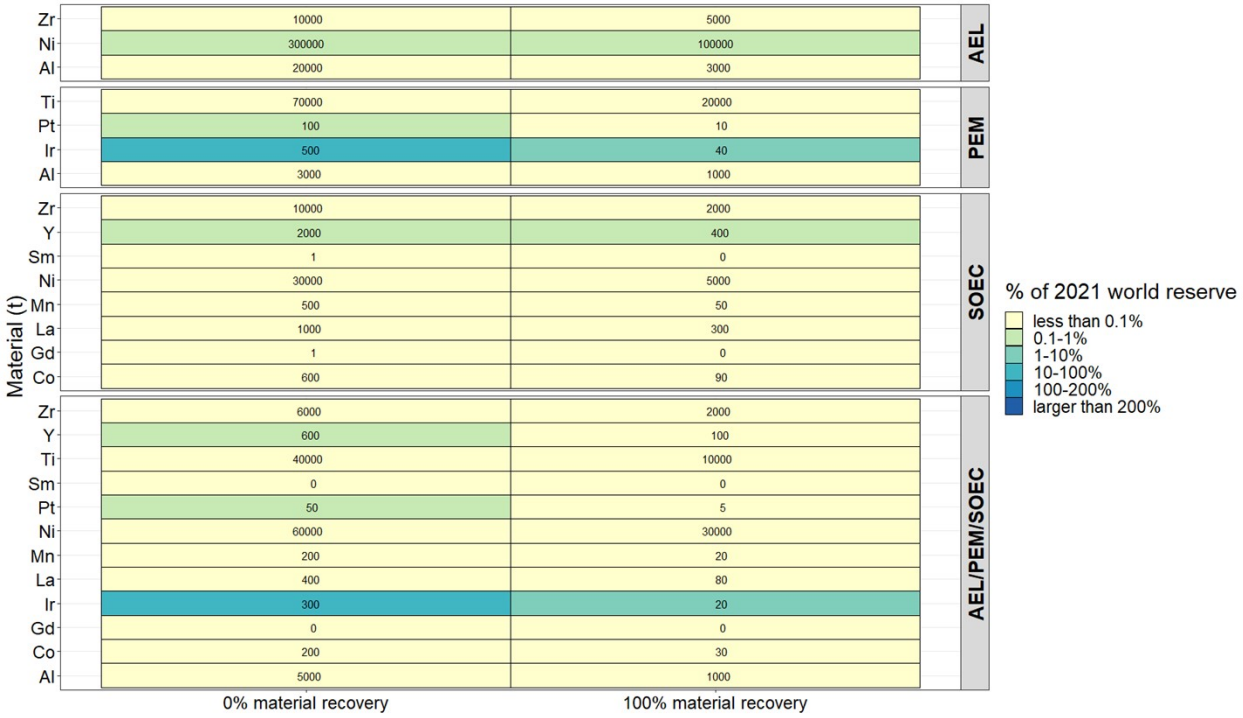

Figure S11 Cumulative demand from 2020 to 2050 for critical materials from water electrolyzers with 0% and 100% material recovery under the high BEV with RE scenario to meet the 2 ˚C climate target with e-gasoline produced from wind electricity. These fleet-level results correspond with Fischer-Tropsch gasoline produced from direct air capture CO_2 and powered by wind electricity and solar thermal heat. The first three panels represent scenarios with 100% of a certain electrolyzer technology, and the last panel represents a scenario with a 20% share of alkaline electrolysis (AEL), 50% of proton exchange membrane (PEM), and 30% of solid oxide electrolyzer cell (SOEC). We include material use for water electrolyzers only for e-gasoline production but not for hydrogen production for fuel cell vehicles. Abbreviations: Al: aluminum; Co: cobalt; Gd: gadolinium; Ir: iridium; La: lanthanum; Mn: manganese; Ni: nickel; Pt: platinum; Sm: Samarium; Ti: titanium; Y: yttrium; Zr: zirconium.

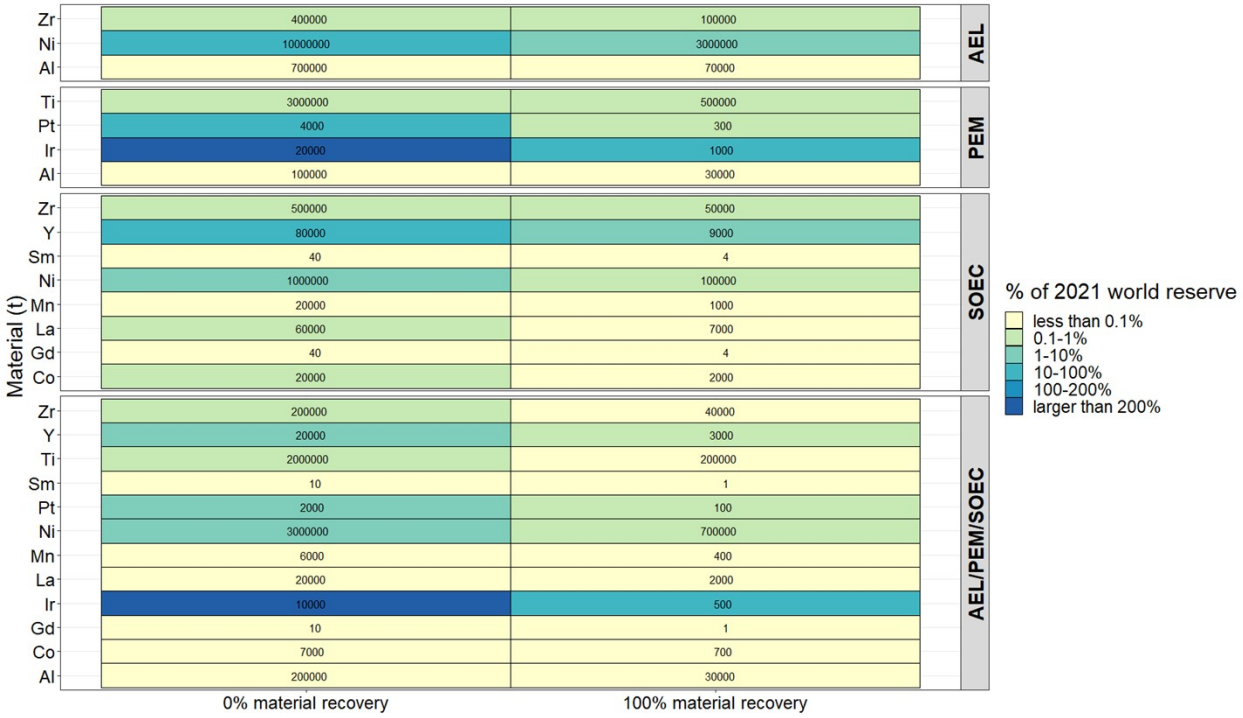

Figure S12 Cumulative demand from 2020 to 2050 for critical materials from water electrolyzers with 0% and 100% material recovery under the BAU BEV with U.S. grid scenario to meet the 1.5 ˚C climate target with e-gasoline produced from solar PV electricity. These fleet-level results correspond with FT-gasoline produced from direct air capture CO_2 and powered by solar photovoltaic (PV) electricity and solar thermal heat. The first three panels represent scenarios with 100% of a certain electrolyzer technology, and the last panel represents a scenario with a 20% share of alkaline electrolysis (AEL), 50% of proton exchange membrane (PEM), and 30% of solid oxide electrolyzer cell (SOEC). We include material use for water electrolyzers only for e-gasoline production but not for hydrogen production for fuel cell vehicles.
Abbreviations: Al: aluminum; Co: cobalt; Gd: gadolinium; Ir: iridium; La: lanthanum; Mn: manganese; Ni: nickel; Pt: platinum; Sm: Samarium; Ti: titanium; Y: yttrium; Zr: zirconium.

3.9.2 Cumulative demand for critical materials from renewable electricity generation

Figure S13 and **Figure S14** present the cumulative demand for critical materials from renewable electricity generation to produce e-gasoline to meet the 2 °C climate target under the BAU BEV with U.S. grid and high BEV with RE scenarios, respectively. **Figure S15** presents the cumulative demand for critical materials from renewable electricity generation to produce e-gasoline to meet the 1.5 °C climate target under the BAU BEV with U.S. grid scenario. Other scenarios are similar to the presented ones and so results are not shown.

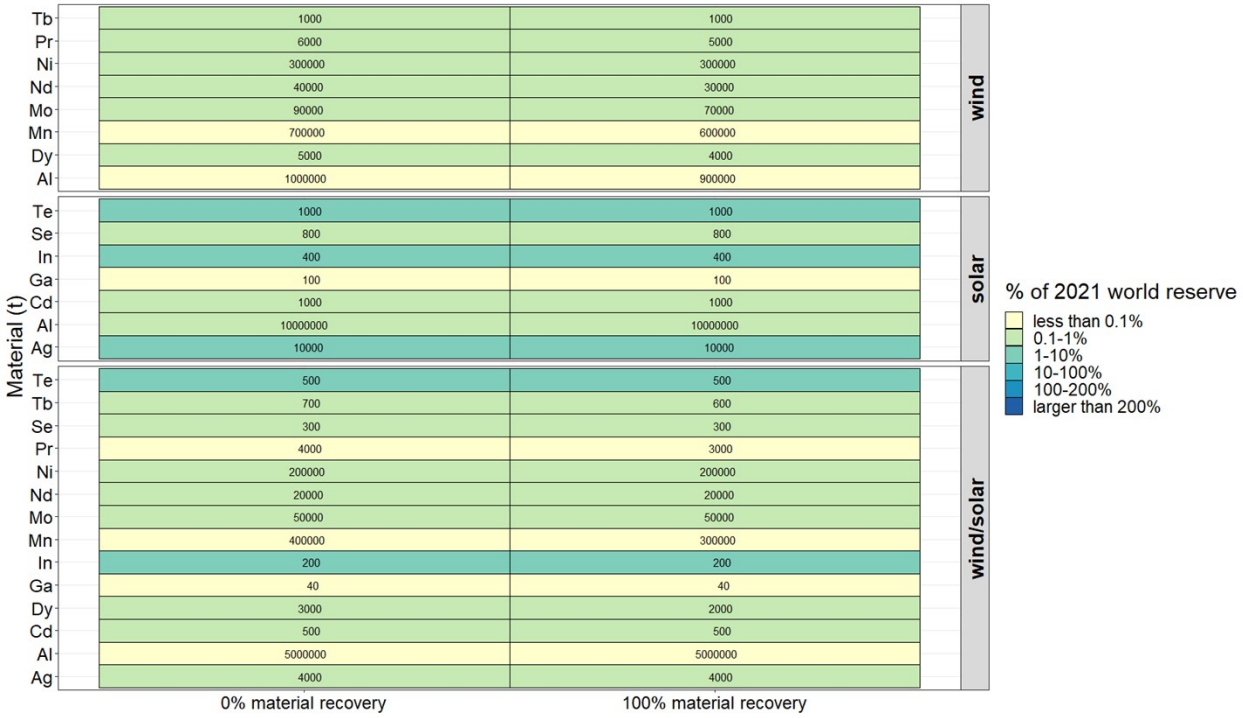

Figure S13 Cumulative demand from 2020 to 2050 for critical materials from renewable electricity generation with 0% and 100% material recovery under the high BEV with U.S. grid scenario to meet the 2 ˚C climate target. These fleet-level results correspond with Fischer-Tropsch gasoline produced from electrolysis or co-electrolysis and CO_2 captured by direct air capture heated by solar thermal energy. The technology share of electrolyzer technology is 20% share of alkaline electrolysis, 50% of proton exchange membrane, and 30% of solid oxide electrolyzer cell. The first two panels represent scenarios with 100% wind or solar photovoltaic (PV) electricity, and the last panel represents a scenario with the assumed source share of wind and solar PV electricity. We include material use for generating renewable electricity only for e-gasoline production but not for vehicle charging.
Abbreviations: Ag: silver; Al: aluminum; Cd: cadmium; Dy: dysprosium; Ga: gallium; In: indium; Mn: manganese; Mo: molybdenum; Nd: neodymium; Ni: nickel; Pr: praseodymium; Se: selenium; Tb: terbium; Te: tellurium.

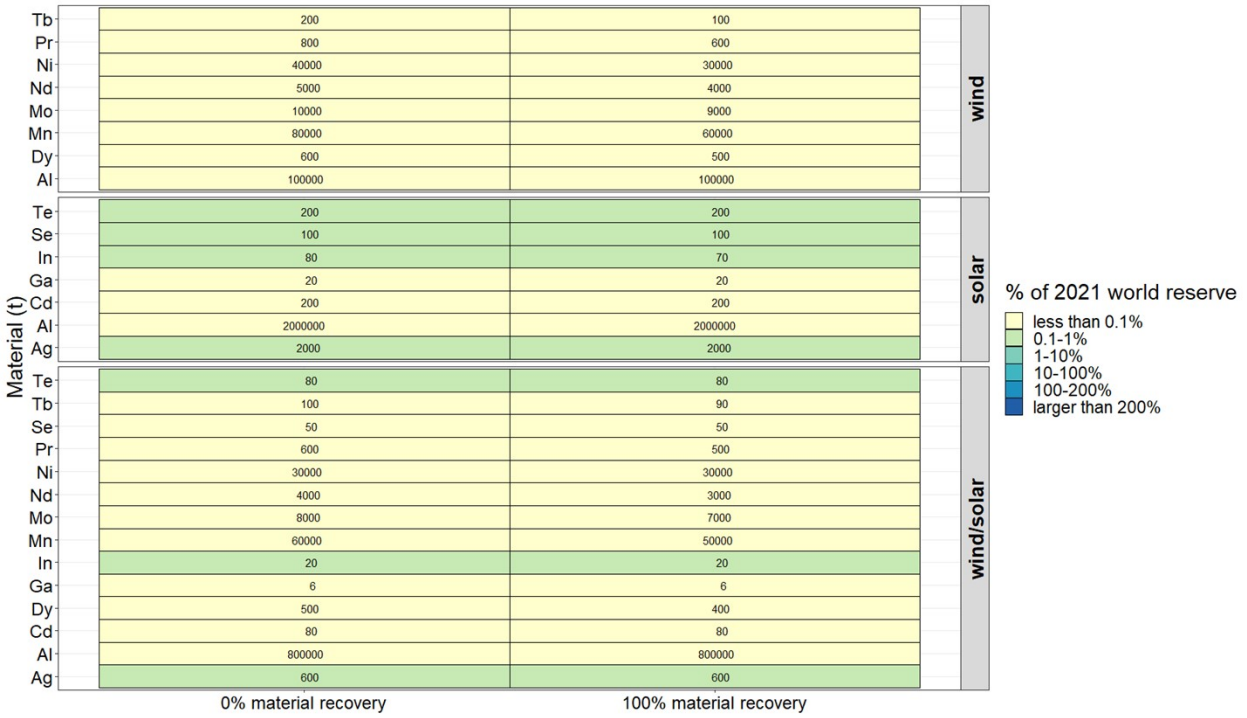

Figure S14 Cumulative demand from 2020 to 2050 for critical materials from renewable electricity generation with 0% and 100% material recovery under the high BEV with RE scenario to meet the 2 ˚C climate target. These fleet-level results correspond with Fischer-Tropsch gasoline produced from electrolysis or co-electrolysis and CO_2 captured by direct air capture heated by solar thermal energy. The technology share of electrolyzer technology is 20% share of alkaline electrolysis, 50% of proton exchange membrane, and 30% of solid oxide electrolyzer cell. The first two panels represent scenarios with 100% wind or solar photovoltaic (PV) electricity, and the last panel represents a scenario with the assumed source share of wind and solar PV electricity. We include material use for generating renewable electricity only for e-gasoline production but not for vehicle charging.
Abbreviations: Ag: silver; Al: aluminum; Cd: cadmium; Dy: dysprosium; Ga: gallium; In: indium; Mn: manganese; Mo: molybdenum; Nd: neodymium; Ni: nickel; Pr: praseodymium; Se: selenium; Tb: terbium; Te: tellurium.

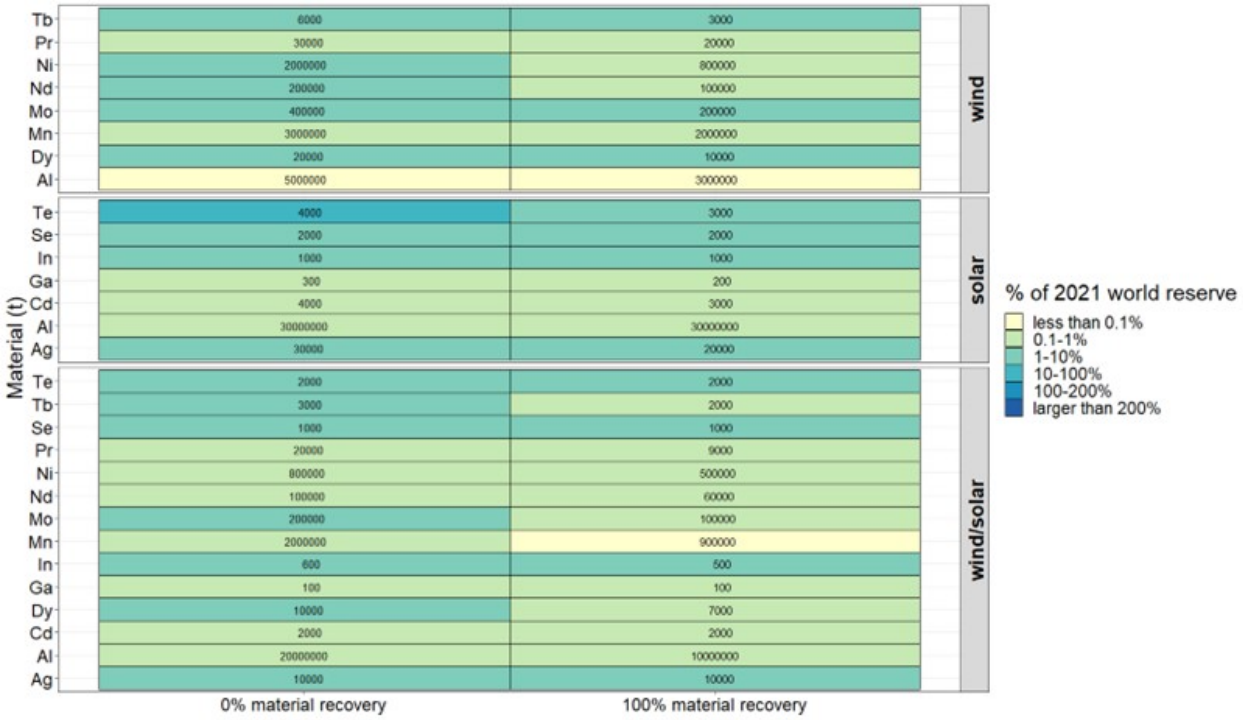

Figure S15 Cumulative demand from 2020 to 2050 for critical materials from renewable electricity generation with 0% and 100% material recovery under the high BEV with U.S. grid scenario to meet the 1.5 ˚C climate target. These fleet-level results correspond with Fischer-Tropsch gasoline produced from electrolysis or co-electrolysis and CO_2 captured by direct air capture heated by solar thermal energy. The technology share of electrolyzer technology is 20% share of alkaline electrolysis, 50% of proton exchange membrane, and 30% of solid oxide electrolyzer cell. The first two panels represent scenarios with 100% wind or solar photovoltaic (PV) electricity, and the last panel represents a scenario with the assumed source share of wind and solar PV electricity. We include material use for generating renewable electricity only for e-gasoline production but not for vehicle charging.
Abbreviations: Ag: silver; Al: aluminum; Cd: cadmium; Dy: dysprosium; Ga: gallium; In: indium; Mn: manganese; Mo: molybdenum; Nd: neodymium; Ni: nickel; Pr: praseodymium; Se: selenium; Tb: terbium; Te: tellurium.

3.9.3 Combined cumulative demand for critical materials from water electrolyzers, renewable electricity generation, and battery manufacturing

Table S29 shows the cumulative demand from 2020 to 2050 for critical materials from battery manufacturing under high BEV scenarios, obtained from Tarabay et al. [83]. High BEV scenarios are assumed to have 100% new sales of BEVs by 2035. We collect data for scenarios with constant market share and 0% or 90% material recovery from [83]. The constant market share is represented by 71% nickel manganese cobalt oxide (NMC) cathode 622, 25% lithium nickel cobalt aluminum oxide (NCA) cathode, and 4% lithium iron phosphate (LFP) cathode in [83].

Table S29 Cumulative demand from 2020 to 2050 for critical materials from battery manufacturing under high BEV scenarios [1] (Source: [83]**)**

Material	Assumptions [2]	Cumulative demand (Mt)
Aluminum (Al)	Constant market share + 0% material recovery	29
	Constant market share + 90% material recovery	22
Cobalt (Co)	Constant market share + 0% material recovery	6
	Constant market share + 90% material recovery	5
Lithium (Li)	Constant market share + 0% material recovery	4
	Constant market share + 90% material recovery	3
Manganese (Mn)	Constant market share + 0% material recovery	5
	Constant market share + 90% material recovery	3
Nickel (Ni)	Constant market share + 0% material recovery	22
	Constant market share + 90% material recovery	16

[1] High BEV scenarios are assumed to have 100% new sales of BEVs by 2035.

[2] Assumptions are obtained from Tarabay et al. [83]. The "Constant market share + 0% material recovery" scenario corresponds to the "No Change (Reference)" scenario in [83], while the "Constant market share + 90% material recovery" scenario corresponds to the "Direct" scenario in [83]. The "constant market share" is represented by 71% nickel manganese cobalt oxide (NMC) cathode 622, 25% lithium nickel cobalt aluminum oxide (NCA) cathode, and 4% lithium iron phosphate (LFP) cathode in [83].

Table S30 presents the cumulative demand for critical materials from water electrolyzers, renewable electricity generation, and battery manufacturing during 2020-2050 to meet 1.5 and 2 °C climate targets under high BEV with U.S. grid scenario. Data for battery manufacturing are collected from Tarabay et al. [83]. Only materials with a demand larger than 1% of the 2021 world reserve without material recovery are presented.

Table S30 Cumulative demand for critical materials from water electrolyzers, renewable electricity generation, and battery manufacturing during 2020-2050 to meet 1.5 and 2 °C climate targets under high BEV with U.S. grid scenario [1]

Climate target	Material	Cumulative demand (t)		% 2021 world reserve	
		No material recovery	With material recovery	No material recovery	With material recovery
1.5 °C	Cobalt (Co)	6200000	4600000	82%	60%
	Iridium (Ir)	4800	470	310%	31%
	Nickel (Ni)	23000000	17000000	25%	18%
	Lithium (Li)	4400000	3200000	20%	15%
	Tellurium (Te)	910	900	2.90%	2.90%
	Indium (In)	280	270	1.80%	1.80%
	Silver (Ag)	7400	7400	1.40%	1.40%
	Molybdenum (Mo)	190000	160000	1.20%	1%
	Yttrium (Y)	11000	2600	3.10%	0.74%
	Platinum (Pt)	920	130	2.80%	0.41%

2 °C	Cobalt (Co)	6200000	4600000	82%	60%
	Nickel (Ni)	22000000	16000000	23%	17%
	Lithium (Li)	4400000	3200000	20%	15%
	Iridium (Ir)	2400	190	160%	12%
	Tellurium (Te)	520	520	1.70%	1.70%
	Indium (In)	170	170	1.10%	1.10%
	Yttrium (Y)	5600	1000	1.60%	0.29%
	Platinum (Pt)	470	53	1.40%	0.16%

[1] The results correspond to Fischer-Tropsch gasoline produced from the assumed market share of electrolyzers and renewable electricity sources, and CO_2 from direct air capture heated by solar thermal energy. Only materials with a demand larger than 1% of the 2021 world reserve without material recovery are presented.

Figure S16 shows the contribution of water electrolyzers, renewable electricity generation, and battery manufacturing to cumulative demand for cobalt, iridium, lithium, and nickel during 2020-2050 to meet 1.5 and 2 °C climate targets under high BEV with U.S. grid scenario.

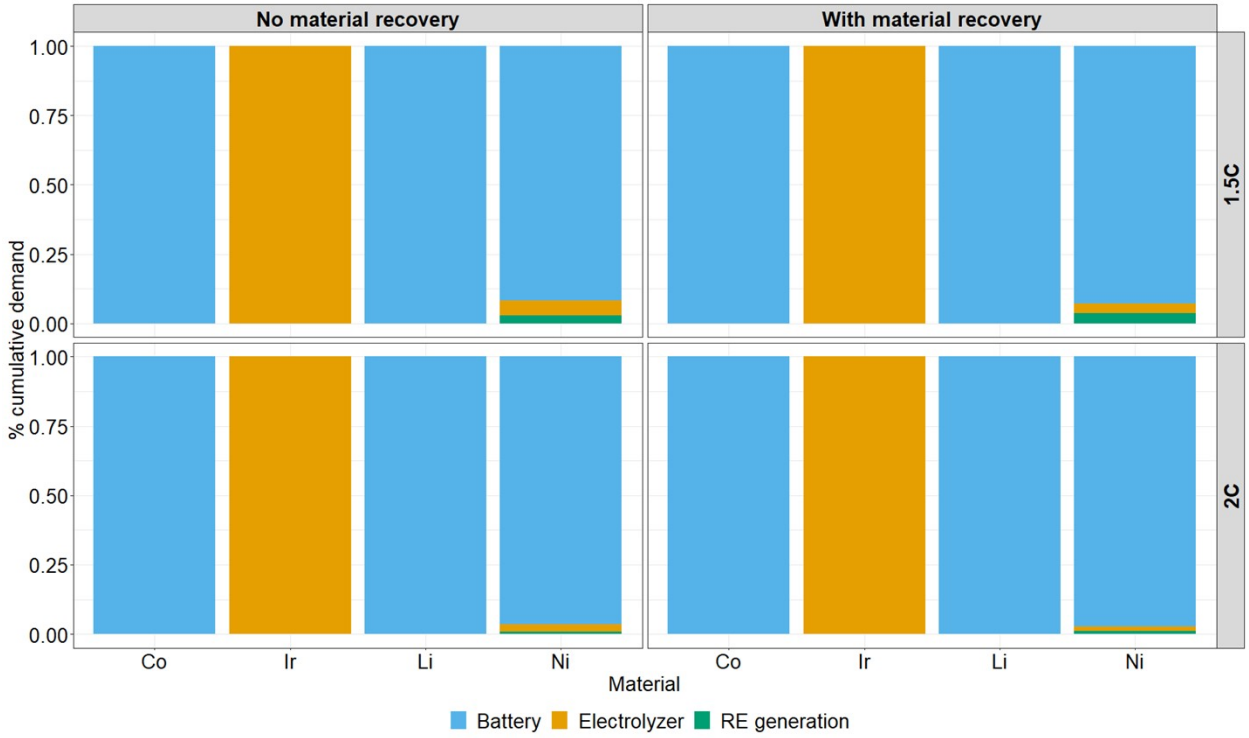

Figure S16 Contribution of water electrolyzers, renewable electricity (RE) generation, and battery manufacturing to cumulative demand for cobalt (Co), iridium (Ir), lithium (Li), and nickel (Ni) during 2020-2050 to meet 1.5 and 2 °C climate targets under high BEV with U.S. grid scenario. The results correspond to Fischer-Tropsch gasoline produced from the assumed market share of electrolyzers and renewable electricity sources, and CO_2 from direct air capture heated by solar thermal energy. The "With material recovery" scenario is represented by a material recovery rate of 90% in battery manufacturing and 100% in electrolyzer and RE generation. Only materials with a demand larger than 10% of the 2021 world reserve without material recovery are presented.

3.10 Production cost and carbon abatement costs of FT-fuels and MTG-gasoline from literature

Figure S17 and **Figure S18** show the production costs of FT-fuels and MTG-gasoline collected from the literature with the unit of USD2022 per MJ of fuel and USD2022 per L of fuel. All reported production costs are higher than the 5-year average production costs of conventional gasoline and diesel during 2018-2022 in the U.S.

The wide range of e-gasoline production costs derives from variations in economic assumptions and production scenarios. For economic assumptions, the production cost is mainly driven by the prices of electricity and CO_2. The lowest cost of \$0.72/L (\$0.023/MJ) is from Ueckerdt et al. [63] whose electricity price was \$0.05/kWh and CO_2 price was \$82/t CO_2, while the highest cost of \$8.3/L (\$0.27/MJ) is from Brynolf et al. [64] whose electricity price was \$0.08/kWh and CO_2 price was \$1600/t CO_2.

For electrolysis and co-electrolysis, it was reported that e-gasoline based on SOEC electrolysis has the lowest cost due to the high production efficiency [11], [64], while e-gasoline based on PEM electrolysis has the highest cost due to the use of noble metals like platinum and iridium [64], [84]. For chemical synthesis, Brynolf et al. [64] reported higher production costs of MTG-gasoline compared to FT-liquids, while Soler et al. [9] reported higher production costs of FT-diesel compared to MTG-gasoline. These studies differ in their conclusions because of the uncertainty of the power-to-fuel efficiency of the two production routes [9], [64]. For carbon capture, capturing CO_2 from industrial flue gas costs \$21-110/t CO_2, which is generally cheaper than the estimated 82-1600/t CO_2 from DAC due to its higher energy consumption [11], [39], [63], [64], [65].

Figure S19 shows the carbon abatement costs of FT-fuels and MTG-gasoline collected from the literature. Some reported carbon abatement costs fall within or below the range of social costs of GHG emitted between 2020 and 2050, indicating that there are social economic benefits to replacing conventional fossil fuels with FT-fuels and MTG-gasoline. **Table S31** summarizes technological and economic assumptions and results for all used scenarios from the literature.

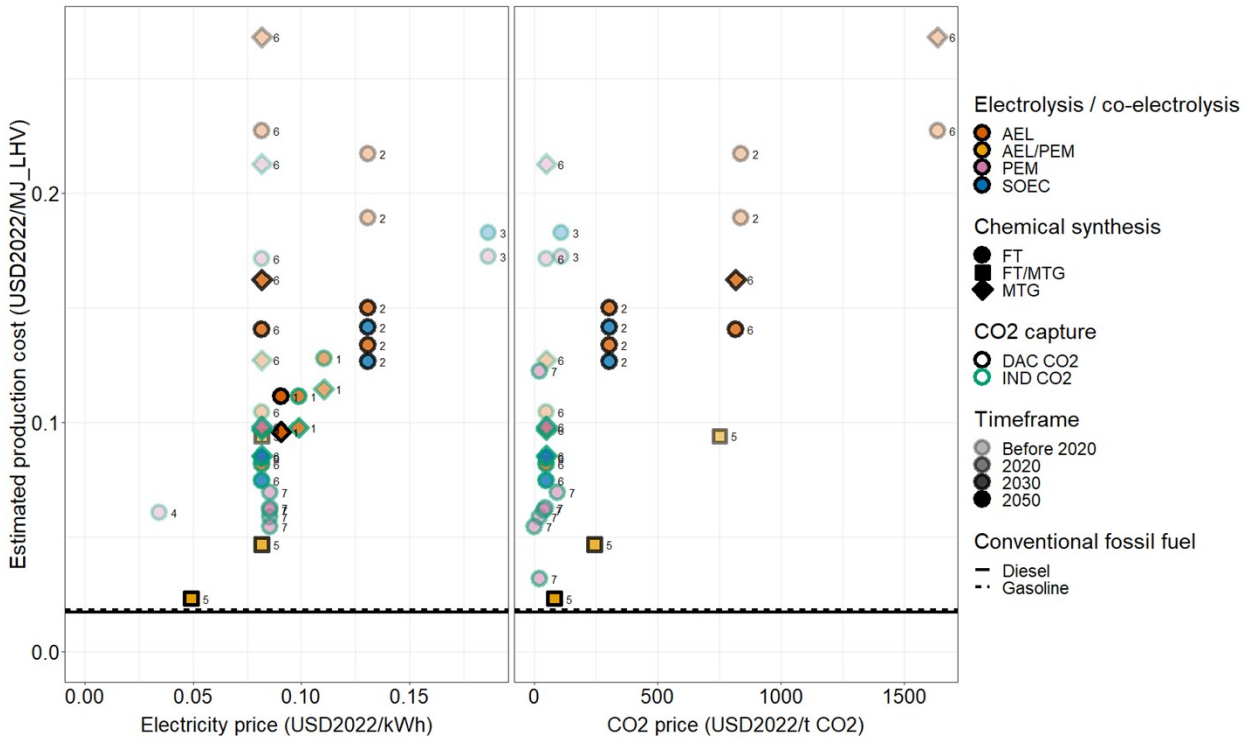

Figure S17 Production cost of FT-fuels and MTG-gasoline in the unit of MJ from literature versus electricity price and CO_2 price. The unit of MJ refers to the lower heating value (LHV) of the fuel. The production costs of conventional diesel and gasoline are the 5-year average crude oil price and refinery cost from 2018 to 2022, which are \$0.017/MJ for diesel and \$0.018/MJ for gasoline. Data comes from U.S. EIA [70], [71]. Ueckderdt et al. (number 5) [63] did not specify whether they used AEL or PEM electrolysis and FT or MTG production pathways, and thus the figure shows "AEL/PEM" and "FT/MTG". The numbering of literature is as follows: 1. Soler et al. [9], 2. Hombach et al. [11], 3. Ordóñez et al. [39], 4. Kannangara et al. [62], 5. Ueckerdt et al. [63], 6. Brynolf et al. [64], and 7. Zang et al. [65].

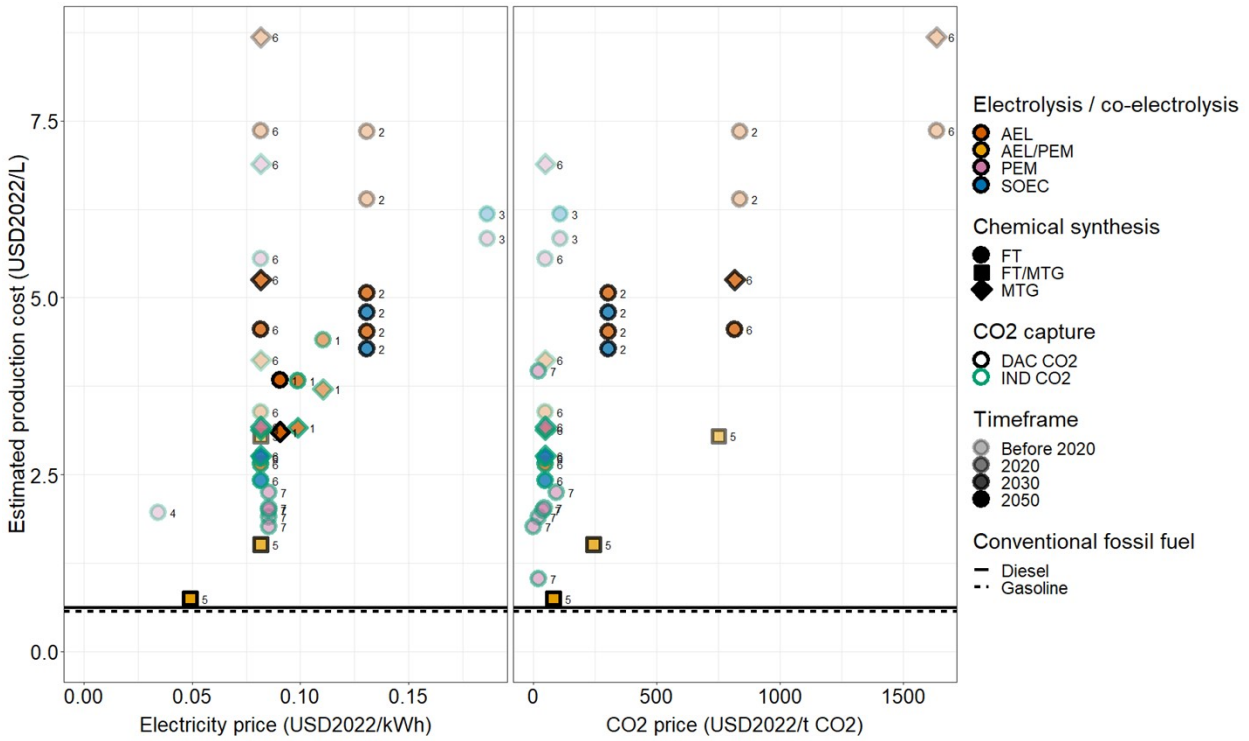

Figure S18 Production cost of FT-fuels and MTG-gasoline in the unit of L from literature versus electricity price and CO_2 price. The production costs of conventional diesel and gasoline are the 5-year average crude oil price and refinery cost from 2018 to 2022, which are $0.61/L for diesel and $0.57/L for gasoline. Data comes from U.S. EIA [70], [71]. Ueckderdt et al. (number 5) [63] did not specify whether they used AEL or PEM electrolysis and FT or MTG production pathways, and thus the figure shows "AEL/PEM" and "FT/MTG". The numbering of literature is as follows: 1. Soler et al. [9], 2. Hombach et al. [11], 3. Ordóñez et al. [39], 4. Kannangara et al. [62], 5. Ueckerdt et al. [63], 6. Brynolf et al. [64], and 7. Zang et al. [65].

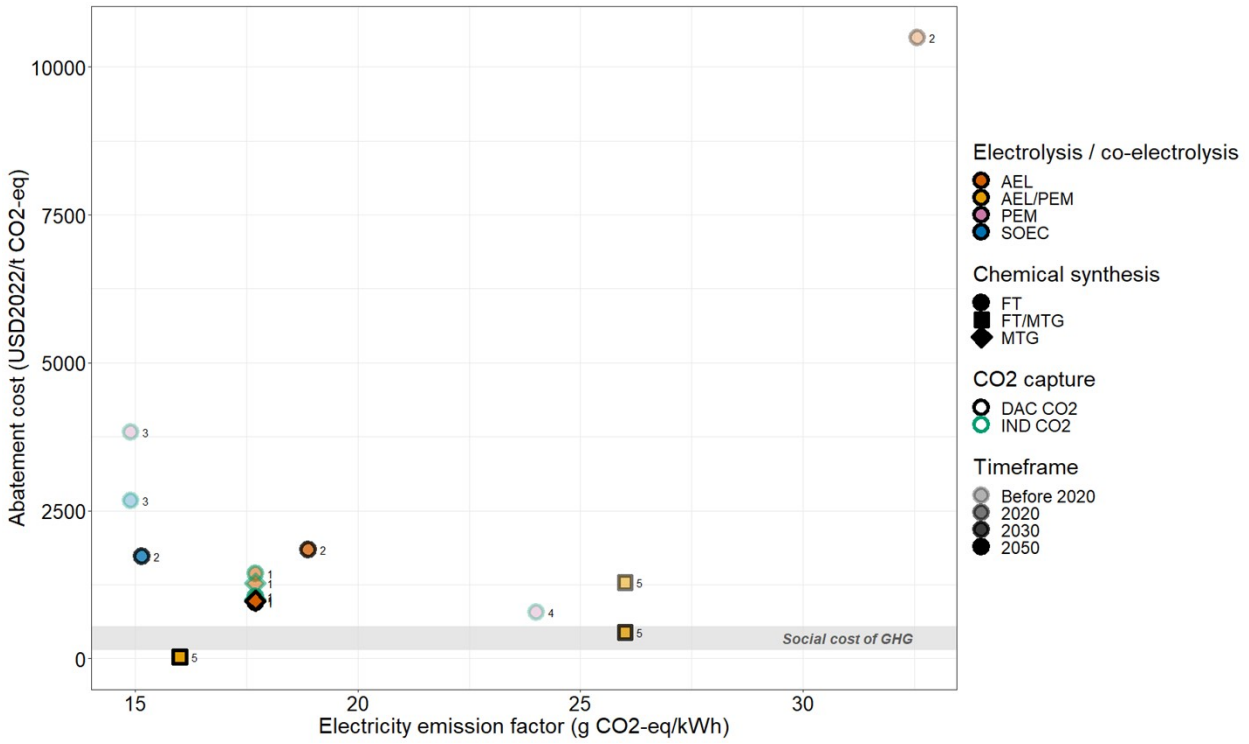

Figure S19 Carbon abatement cost of FT-fuels and MTG-gasoline versus electricity emission factor. The social costs of carbon come from the U.S. EPA [72]. The figure shows the minimum and maximum values of GHG emitted during 2020-2050. The values range from \$140/t CO_2 to \$540/t CO_2 (USD2022). Ueckderdt et al. (number 5) [63] did not specify whether they used AEL or PEM electrolysis and FT or MTG production pathways, and thus the figure shows "AEL/PEM" and "FT/MTG". The numbering of literature is as follows: 1. Soler et al. [9], 2. Hombach et al. [11], 3. Ordóñez et al. [39], 4. Kannangara et al. [62], and 5. Ueckerdt et al. [63].

Table S31 Production costs, abatement costs, and technological and economic assumptions from the literature

Source number	Source	Timeframe	E-fuel type	Production pathway	Electricity price (USD2022/kWh)	CO_2 price (USD2022/t CO2)	Total cost (USD2022/MJ_LHV)	Total cost (USD2022/L)	Electricity EF (g CO2-eq/kWh)	Total emission (g CO_2-eq/MJ_LHV)	Abatement cost (USD2022/t CO_2-eq)
6	Brynolf et al.	Before 2020	MTG-gasoline	AEL+MTG+DAC CO2	0.082	1600	0.27	8.3	NA	NA	NA
6	Brynolf et al.	Before 2020	FT-liquids	AEL+FT+DAC CO2	0.082	1600	0.23	7	NA	NA	NA
2	Hombach et al.	Before 2020	FT-diesel	AEL+FT+DAC CO2	0.13	840	0.22	7.3	33	64	11000
6	Brynolf et al.	Before 2020	MTG-gasoline	PEM+MTG+IND CO2	0.082	49	0.21	6.6	NA	NA	NA
2	Hombach et al.	Before 2020	FT-diesel	AEL+FT+DAC CO2	0.13	840	0.19	6.4	650	440	-500
3	Ordóñez et al.	Before 2020	FT-gasoline	SOEC+FT+IND CO2	0.19	110	0.18	6.2	15	-45	2700
3	Ordóñez et al.	Before 2020	FT-gasoline	PEM+FT+IND CO2	0.19	110	0.17	5.8	15	-24	3800
6	Brynolf et al.	Before 2020	FT-liquids	PEM+FT+IND CO2	0.082	49	0.17	5.3	NA	NA	NA
6	Brynolf et al.	2030	MTG-gasoline	AEL+MTG+DAC CO2	0.082	820	0.16	5	NA	NA	NA
2	Hombach et al.	2030	FT-diesel	AEL+FT+DAC CO2	0.13	300	0.15	5.1	19	7.7	1800
2	Hombach et al.	2030	FT-diesel	SOEC+FT+DAC CO2	0.13	300	0.14	4.8	15	6.6	1700
6	Brynolf et al.	2030	FT-liquids	AEL+FT+DAC CO2	0.082	820	0.14	4.3	NA	NA	NA
2	Hombach et al.	2030	FT-diesel	AEL+FT+DAC CO2	0.13	300	0.13	4.5	370	150	-2100
7	Zang et al.	2020	FT-diesel	PEM+FT+IND CO2	NA	21	0.13	4	NA	NA	NA
1	Soler et al.	2020	FT-diesel	AEL+FT+IND CO2	0.11	NA	0.13	4.4	18	13	1400
6	Brynolf et al.	Before 2020	MTG-gasoline	AEL+MTG+IND CO2	0.082	49	0.13	3.9	NA	NA	NA
2	Hombach et al.	2030	FT-diesel	SOEC+FT+DAC CO2	0.13	300	0.13	4.3	370	110	-7300
1	Soler et al.	2020	MTG-	AEL+MTG+IND CO2	0.11	NA	0.11	3.5	18	12	1300

			gasoline								
1	Soler et al.	2050	FT-diesel	AEL+FT+DAC CO2	0.091	NA	0.11	3.8	18	13	940
1	Soler et al.	2030	FT-diesel	AEL+FT+IND CO2	0.099	NA	0.11	3.8	18	12	1000
6	Brynolf et al.	Before 2020	FT-liquids	AEL+FT+IND CO2	0.082	49	0.1	3.2	NA	NA	NA
6	Brynolf et al.	2030	MTG-gasoline	PEM+MTG+IND CO2	0.082	49	0.098	3	NA	NA	NA
1	Soler et al.	2030	MTG-gasoline	AEL+MTG+IND CO2	0.099	NA	0.098	3	18	11	1000
6	Brynolf et al.	2030	MTG-gasoline	AEL+MTG+IND CO2	0.082	49	0.097	3	NA	NA	NA
1	Soler et al.	2050	MTG-gasoline	AEL+MTG+DAC CO2	0.091	NA	0.096	3	18	12	970
5	Ueckerdt et al.	2020	E-gasoline	AEL/PEM+FT/MTG+DAC CO2	0.082	750	0.094	2.9	26	NA	1300
6	Brynolf et al.	2030	MTG-gasoline	SOEC+MTG+IND CO2	0.082	49	0.085	2.6	NA	NA	NA
6	Brynolf et al.	2030	FT-liquids	PEM+FT+IND CO2	0.082	49	0.084	2.6	NA	NA	NA
6	Brynolf et al.	2030	FT-liquids	AEL+FT+IND CO2	0.082	49	0.082	2.5	NA	NA	NA
6	Brynolf et al.	2030	FT-liquids	SOEC+FT+IND CO2	0.082	49	0.075	2.3	NA	NA	NA
7	Zang et al.	2020	FT-diesel	PEM+FT+IND CO2	0.085	93	0.073	2.3	NA	NA	NA
7	Zang et al.	2020	FT-diesel	PEM+FT+IND CO2	0.085	47	0.066	2	NA	NA	NA
7	Zang et al.	2020	FT-diesel	PEM+FT+IND CO2	0.085	41	0.065	2	NA	NA	NA
4	Kannangara et al.	Before 2020	FT-diesel	PEM+FT+IND CO2	0.034	NA	0.064	2	24	32	780
7	Zang et al.	2020	FT-diesel	PEM+FT+IND CO2	0.085	21	0.061	1.9	NA	NA	NA
7	Zang et al.	2020	FT-diesel	PEM+FT+IND CO2	0.085	0	0.057	1.8	NA	NA	NA
5	Ueckerdt et al.	2030	E-gasoline	AEL/PEM+FT/MTG+DAC CO2	0.082	250	0.047	1.4	26	32	450
7	Zang et al.	2020	FT-diesel	PEM+FT+IND CO2	NA	21	0.033	1	NA	NA	NA
5	Ueckerdt et al.	2050	E-gasoline	AEL/PEM+FT/MTG+DAC CO2	0.049	82	0.023	0.72	16	24	31

* The numbering of literature is as follows: 1. Soler et al. [9], 2. Hombach et al. [11], 3. Ordóñez et al. [39], 4. Kannangara et al. [62], 5. Ueckerdt et al. [63], 6. Brynolf et al. [64] and 7. Zang et al. [65].
Abbreviations: AEL: alkaline electrolysis; PEM: proton exchange membrane electrolysis; SOEC: solid oxide electrolyzer cell; FT: Fischer-Tropsch; MTG: methanol-to-gasoline; DAC: direct air capture; IND: industrial flue gas; EF: emission factor; NA: not applicable or no available data.

3.11 Comparing tailpipe emissions of air pollutants from combusting e-gasoline and conventional gasoline in ICEVs-G

This section provides more details on the two studies that examined single Euro vehicles using e-gasoline and compared results with those using conventional gasoline [85], [86]. Transport & Environment [85] compared tailpipe emissions from using high paraffinic e-gasoline (representing products from FT synthesis) and standard E10 European Union petrol in a Mercedes A180 (a Euro 6d-temp, 4-cylinder, 1.3 L, 6-speed manual car fitted with a gasoline particulate filter) through official lab tests and real-world lab tests. Results showed that using e-gasoline would result in 1.2-3 times higher emissions of CO, 81-97% lower emissions of the number of particles larger than 10 nm (PN10), and no significant differences in emissions of NO_X and particle mass [85]. Demuynck et al. [86] compared the tailpipe emissions between using MTG-gasoline and RON95 E10 gasoline in a Euro 6d C-segment car (4-cylinder, 1.5 L) installed with an advanced emission control system. They observed slightly lower emissions of NOx, PN10, and non-methane organic gases for MTG-gasoline but concluded the emissions are similar [86].

References

[1] S. Searle and A. Christensen, “Decarbonization potential of electrofuels in the European Union.” [Online]. Available: https://theicct.org/publications/decarbonization-potential-electrofuels-eu

[2] M. Rottoli, A. Dirnaichner, R. Pietzcker, F. Schreyer, and G. Luderer, “Alternative electrification pathways for light-duty vehicles in the European transport sector,” *Transp Res D Transp Environ*, vol. 99, p. 103005, 2021, doi: 10.1016/j.trd.2021.103005.

[3] A. Dirnaichner *et al.*, “Life-cycle impacts from different decarbonization pathways for the European car fleet,” *Environmental Research Letters*, vol. 17, no. 4, p. 44009, 2022, doi: 10.1088/1748-9326/ac4fdb.

[4] M. Rüdisüli *et al.*, “Prospective life-cycle assessment of greenhouse gas emissions of electricity-based mobility options,” *Appl Energy*, vol. 306, p. 118065, 2022, doi: 10.1016/j.apenergy.2021.118065.

[5] A. Garcia, J. Monsalve-Serrano, D. Villalta, and S. Tripathi, “Electric Vehicles vs e-Fuelled ICE Vehicles: Comparison of potentials for Life Cycle CO2 Emission Reduction,” Mar. 2022. doi: 10.4271/2022-01-0745.

[6] Princeton University, “Net-Zero America Project.” Accessed: Mar. 18, 2023. [Online]. Available: https://netzeroamerica.princeton.edu/?explorer=pathway&state=national&table=e-positive&limit=200

[7] B. Helgeson and J. Peter, “The role of electricity in decarbonizing European road transport – Development and assessment of an integrated multi-sectoral model,” *Appl Energy*, vol. 262, p. 114365, 2020, doi: 10.1016/j.apenergy.2019.114365.

[8] ANL, “The Greenhouse Gases, Regulated Emissions, and Energy Use in Technologies (GREET®) Model, Version 2022,” Oct. 2022, *Argonne National Laboratory*: 2022. Accessed: Dec. 16, 2022. [Online]. Available: https://greet.es.anl.gov/greet_excel_model.models

[9] A. Soler *et al.*, “E-Fuels: A techno-economic assessment of European domestic production and imports towards 2050 (Concawe Report 17/22),” Brussels, Nov. 2022. Accessed: Mar. 16, 2023. [Online]. Available: https://www.concawe.eu/publication/e-fuels-a-techno-economic-assessment-of-european-domestic-production-and-imports-towards-2050/

[10] U.S. EIA, “Annual Energy Outlook 2022 with projections to 2050,” 2022. [Online]. Available: https://www.eia.gov/outlooks/aeo/

[11] L. E. Hombach, L. Doré, K. Heidgen, H. Maas, T. J. Wallington, and G. Walther, “Economic and environmental assessment of current (2015) and future (2030) use of E-fuels in light-duty vehicles in Germany,” *J Clean Prod*, vol. 207, no. 6, pp. 153–162, 2019, doi: 10.1016/j.jclepro.2018.09.261.

[12] C. van der Giesen, R. Kleijn, and G. J. Kramer, “Energy and Climate Impacts of Producing Synthetic Hydrocarbon Fuels from CO2,” *Environ Sci Technol*, vol. 48, no. 12, pp. 7111–7121, 2014, doi: 10.1021/es500191g.

[13] U.S. EIA, “How much electricity is lost in electricity transmission and distribution in the United States?,” U.S. Energy Information Administration. Accessed: Apr. 06, 2023. [Online]. Available: https://www.eia.gov/tools/faqs/faq.php?id=105&t=3

[14] Oak Ridge National Laboratory, “Where the Energy Goes: Electric Cars.” Accessed: Apr. 06, 2023. [Online]. Available: https://www.fueleconomy.gov/feg/atv-ev.shtml

[15] Oak Ridge National Laboratory, “Where the Energy Goes: Hybrids.” Accessed: Apr. 06, 2023. [Online]. Available: https://www.fueleconomy.gov/feg/atv-hev.shtml

[16] Oak Ridge National Laboratory, “Where the Energy Goes: Gasoline Vehicles.” Accessed: Apr. 06, 2023. [Online]. Available: https://www.fueleconomy.gov/feg/atv.shtml

[17] H. Lohse-Busch *et al.*, “Automotive fuel cell stack and system efficiency and fuel consumption based on vehicle testing on a chassis dynamometer at minus 18 °C to positive 35 °C temperatures,” *Int J Hydrogen Energy*, vol. 45, no. 1, pp. 861–872, Jan. 2020, doi: 10.1016/J.IJHYDENE.2019.10.150.

[18] A. Milovanoff, L. Minet, L. Cheah, I. D. Posen, H. L. MacLean, and R. Balasubramanian, “Greenhouse Gas Emission Mitigation Pathways for Urban Passenger Land Transport under Ambitious Climate Targets,” *Environ Sci Technol*, May 2021, doi: 10.1021/acs.est.0c06671.

[19] M. J. Gidden *et al.*, “Global emissions pathways under different socioeconomic scenarios for use in CMIP6: a dataset of harmonized emissions trajectories through the end of the century,” *Geoscientific Model Development Discussions*, no. November, pp. 1–42, 2018, doi: 10.5194/gmd-2018-266.

[20] A. Meyer, *Contraction & convergence: the global solution to climate change*. Green Books, 2000.

[21] U.S. EPA, “Inventory of U.S. Greenhouse Gas Emissions and Sinks: 1990-2021,” Apr. 2023. Accessed: Jun. 24, 2023. [Online]. Available:

https://www.epa.gov/ghgemissions/inventory-us-greenhouse-gas-emissions-andsinks-1990-2021

[22] A. Milovanoff, I. D. Posen, and H. L. MacLean, “Electrification of light-duty vehicle fleet alone will not meet mitigation targets,” *Nat Clim Chang*, vol. 10, no. 12, pp. 1102–1107, 2020, doi: 10.1038/s41558-020-00921-7.

[23] A. Milovanoff, H. L. MacLean, A. F. N. Abdul-Manan, and I. D. Posen, “Does the metric matter? Climate change impacts of light-duty vehicle electrification in the US,” *Environmental Research: Infrastructure and Sustainability*, vol. 2, no. 3, p. 035007, Sep. 2022, doi: 10.1088/2634-4505/ac8071.

[24] H. D. Matthews *et al.*, “Estimating Carbon Budgets for Ambitious Climate Targets,” *Curr Clim Change Rep*, vol. 3, no. 1, pp. 69–77, Mar. 2017, doi: 10.1007/s40641-017-0055-0.

[25] U.S. EIA, “Total Energy Annual Data,” U.S. Energy Information Administration. Accessed: Dec. 17, 2022. [Online]. Available: https://www.eia.gov/totalenergy/data/annual/index.php

[26] bp, “Statistical Review of World Energy (2022),” bp. Accessed: Dec. 17, 2022. [Online]. Available: https://www.bp.com/en/global/corporate/energy-economics/statistical-review-of-world-energy.html

[27] H. F. Williamson, R. L. Andreano, and C. Menezes, “The American Petroleum Industry,” in *Output, Employment, and Productivity in the United States after 1800*, 1966, pp. 349–404. Accessed: Dec. 17, 2022. [Online]. Available: https://www.nber.org/system/files/chapters/c1572/c1572.pdf

[28] A. Odenweller, F. Ueckerdt, G. F. Nemet, M. Jensterle, and G. Luderer, “Probabilistic feasibility space of scaling up green hydrogen supply,” *Nature Energy 2022 7:9*, vol. 7, no. 9, pp. 854–865, Sep. 2022, doi: 10.1038/s41560-022-01097-4.

[29] A. Badgett *et al.*, “Water Electrolyzers and Fuel Cells Supply Chain - Supply Chain Deep Dive Assessment,” Feb. 2022. doi: 10.2172/1871559.

[30] S. Kiemel, T. Smolinka, F. Lehner, J. Full, A. Sauer, and R. Miehe, “Critical materials for water electrolysers at the example of the energy transition in Germany,” *Int J Energy Res*, vol. 45, no. 7, pp. 9914–9935, Jun. 2021, doi: 10.1002/er.6487.

[31] IEA, “The Role of Critical World Energy Outlook Special Report Minerals in Clean Energy Transitions,” 2022. Accessed: Aug. 23, 2022. [Online]. Available: https://iea.blob.core.windows.net/assets/ffd2a83b-8c30-4e9d-980a-52b6d9a86fdc/TheRoleofCriticalMineralsinCleanEnergyTransitions.pdf

[32] J. Koj, C. Wulf, A. Schreiber, and P. Zapp, “Site-Dependent Environmental Impacts of Industrial Hydrogen Production by Alkaline Water Electrolysis,” *Energies (Basel)*, vol. 10, no. 7, p. 860, Jun. 2017, doi: 10.3390/en10070860.

[33] N. T. Nassar and S. M. Fortier, “Methodology and technical input for the 2021 review and revision of the U.S. Critical Minerals List,” in *U.S. Geological Survey Open-File Report 2021–1045*, U.S. Geological Survey, 2021. doi: 10.3133/OFR20211045.

[34] S. Shiva Kumar and V. Himabindu, “Hydrogen production by PEM water electrolysis – A review,” *Mater Sci Energy Technol*, vol. 2, no. 3, pp. 442–454, Dec. 2019, doi: 10.1016/j.mset.2019.03.002.

[35] A. Valente, M. Martín-Gamboa, D. Iribarren, and J. Dufour, “Existing end-of-life technologies applicable to FCH products (D2.2.-V4),” Mar. 2018. Accessed: Aug. 29, 2022. [Online]. Available: http://hytechcycling.eu/wp-content/uploads/d2-2-report-on-existing-recycling-technologies-applicable-to-fch-products.pdf

[36] A. M. Moschovi, E. Zagoraiou, E. Polyzou, and I. Yakoumis, “Recycling of Critical Raw Materials from Hydrogen Chemical Storage Stacks (PEMWE), Membrane Electrode Assemblies (MEA) and Electrocatalysts,” *IOP Conf Ser Mater Sci Eng*, vol. 1024, no. 1, p. 012008, Jan. 2021, doi: 10.1088/1757-899X/1024/1/012008.

[37] S. Häfele, M. Hauck, and J. Dailly, “Life cycle assessment of the manufacture and operation of solid oxide electrolyser components and stacks,” *Int J Hydrogen Energy*, vol. 41, no. 31, pp. 13786–13796, Aug. 2016, doi: 10.1016/J.IJHYDENE.2016.05.069.

[38] S. Sarner *et al.*, “Recycling Strategies for Solid Oxide Cells,” *Adv Energy Mater*, p. 2201805, Jul. 2022, doi: 10.1002/AENM.202201805.

[39] D. F. Ordóñez, N. Shah, and G. Guillén-Gosálbez, “Economic and full environmental assessment of electrofuels via electrolysis and co-electrolysis considering externalities,” *Appl Energy*, vol. 286, p. 116488, 2021, doi: 10.1016/j.apenergy.2021.116488.

[40] H. A. Miller *et al.*, “Green hydrogen from anion exchange membrane water electrolysis: a review of recent developments in critical materials and operating conditions,” *Sustain Energy Fuels*, vol. 4, no. 5, pp. 2114–2133, May 2020, doi: 10.1039/C9SE01240K.

[41] IRENA, “Green hydrogen cost reduction,” Dec. 2020. Accessed: Aug. 23, 2022. [Online]. Available: /publications/2020/Dec/Green-hydrogen-cost-reduction

[42] O. Schmidt, A. Gambhir, I. Staffell, A. Hawkes, J. Nelson, and S. Few, “Future cost and performance of water electrolysis: An expert elicitation study,” *Int J Hydrogen Energy*, vol. 42, no. 52, pp. 30470–30492, Dec. 2017, doi: 10.1016/J.IJHYDENE.2017.10.045.

[43] K. Bareiß, C. de la Rua, M. Möckl, and T. Hamacher, “Life cycle assessment of hydrogen from proton exchange membrane water electrolysis in future energy systems,” *Appl Energy*, vol. 237, pp. 862–872, Mar. 2019, doi: 10.1016/J.APENERGY.2019.01.001.

[44] N. Preux, A. Rolle, and R. N. Vannier, “Electrolytes and ion conductors for solid oxide fuel cells (SOFCs),” in *Functional Materials for Sustainable Energy Applications*, Woodhead Publishing, 2012, ch. 12, pp. 370–401. doi: 10.1533/9780857096371.3.370.

[45] S. C. Singhal and K. Kendall, “Introduction to SOFCs,” in *High-temperature Solid Oxide Fuel Cells: Fundamentals, Design and Applications*, Elsevier Science, 2003, ch. 1, pp. 1–22. doi: 10.1016/B978-185617387-2/50018-0.

[46] American Elements, “8% Yttria Stabilized Zirconia,” American Elements. Accessed: Mar. 18, 2024. [Online]. Available: https://www.americanelements.com/8-yttria-stabilized-zirconia-114168-16-0

[47] A. R. Hanifi, M. A. Laguna-Bercero, N. K. Sandhu, T. H. Etsell, and P. Sarkar, “Tailoring the Microstructure of a Solid Oxide Fuel Cell Anode Support by Calcination and Milling of YSZ,” *Scientific Reports 2016 6:1*, vol. 6, no. 1, pp. 1–9, Jun. 2016, doi: 10.1038/srep27359.

[48] U.S. DOE, “Critical Materials Assessment 2023,” Jul. 2023. Accessed: Jul. 30, 2023. [Online]. Available: https://www.energy.gov/eere/articles/us-department-energy-releases-2023-critical-materials-assessment-evaluate-supply

[49] S. Carrara, P. Alves Dias, B. Plazzotta, and C. Pavel, *Raw materials demand for wind and solar PV technologies in the transition towards a decarbonised energy system*. Publications Office of the European Union, 2020. doi: 10.2760/160859.

[50] A. Elshkaki and T. E. Graedel, “Dynamic analysis of the global metals flows and stocks in electricity generation technologies,” *J Clean Prod*, vol. 59, pp. 260–273, Nov. 2013, doi: 10.1016/j.jclepro.2013.07.003.

[51] N. T. Nassar, D. R. Wilburn, and T. G. Goonan, “Byproduct metal requirements for U.S. wind and solar photovoltaic electricity generation up to the year 2040 under various Clean Power Plan scenarios,” *Appl Energy*, vol. 183, pp. 1209–1226, Dec. 2016, doi: 10.1016/j.apenergy.2016.08.062.

[52] Z. Cao *et al.*, “Resourcing the Fairytale Country with Wind Power: A Dynamic Material Flow Analysis,” *Environ Sci Technol*, vol. 53, no. 19, Oct. 2019, doi: 10.1021/acs.est.9b03765.

[53] NREL, “Electricity Annual Technology Baseline (ATB) Data,” National Renewable Energy Laboratory. Accessed: Oct. 24, 2023. [Online]. Available: https://atb.nrel.gov/electricity/2022/data

[54] P. Wang, L.-Y. Chen, J.-P. Ge, W. Cai, and W.-Q. Chen, “Incorporating critical material cycles into metal-energy nexus of China’s 2050 renewable transition,” *Appl Energy*, vol. 253, Nov. 2019, doi: 10.1016/j.apenergy.2019.113612.

[55] USGS, “Mineral commodity summaries 2022,” 2022. doi: 10.3133/MCS2022.

[56] NRCan, “Aluminum facts,” Natural Resources Canada. Accessed: Oct. 23, 2024. [Online]. Available: https://natural-resources.canada.ca/our-natural-resources/minerals-mining/mining-data-statistics-and-analysis/minerals-metals-facts/aluminum-facts/20510

[57] USGS, “Rare Earths Statistics and Information,” 2021. Accessed: Jan. 25, 2023. [Online]. Available: https://www.usgs.gov/centers/national-minerals-information-center/rare-earths-statistics-and-information

[58] E. Dominish, N. Florin, and S. Teske, “Responsible minerals sourcing for renewable energy,” 2019. Accessed: Oct. 24, 2023. [Online]. Available: https://earthworks.org/wp-content/uploads/2019/04/Responsible-minerals-sourcing-for-renewable-energy-MCEC_UTS_Earthworks-Report.pdf

[59] J. Emsley, *Nature’s building blocks : everything you need to know about the elements*. Oxford ; New York: Oxford University Press, 2011.

[60] USGS, “Platinum-Group Metals,” in *Minerals Yearbook 2019*, U.S. Geological Survey, 2021. Accessed: Aug. 23, 2022. [Online]. Available: https://www.usgs.gov/centers/national-minerals-information-center/platinum-group-metals-statistics-and-information

[61] A. E. Hughes, N. Haque, S. A. Northey, and S. Giddey, “Platinum Group Metals: A Review of Resources, Production and Usage with a Focus on Catalysts,” *Resources 2021, Vol. 10, Page 93*, vol. 10, no. 9, p. 93, Sep. 2021, doi: 10.3390/RESOURCES10090093.

[62] M. Kannangara *et al.*, “A standardized methodology for economic and carbon footprint assessment of CO2 to transport fuels: Comparison of novel bicarbonate electrolysis with competing pathways,” *Appl Energy*, vol. 325, p. 119897, Nov. 2022, doi: 10.1016/J.APENERGY.2022.119897.

[63] F. Ueckerdt, C. Bauer, A. Dirnaichner, J. Everall, R. Sacchi, and G. Luderer, “Potential and risks of hydrogen-based e-fuels in climate change mitigation,” *Nat Clim Chang*, vol. 11, no. 5, pp. 384–393, 2021, doi: 10.1038/s41558-021-01032-7.

[64] S. Brynolf, M. Taljegard, M. Grahn, and J. Hansson, “Electrofuels for the transport sector: A review of production costs,” *Renewable and Sustainable Energy Reviews*, vol. 81, pp. 1887–1905, Jan. 2018, doi: 10.1016/J.RSER.2017.05.288.

[65] G. Zang, P. Sun, A. A. Elgowainy, A. Bafana, and M. Wang, “Performance and cost analysis of liquid fuel production from H2 and CO2 based on the Fischer-Tropsch process,” *Journal of CO2 Utilization*, vol. 46, p. 101459, Apr. 2021, doi: 10.1016/J.JCOU.2021.101459.

[66] OECD, “Purchasing Power Parities - Frequently Asked Questions (FAQs).” Accessed: Apr. 08, 2023. [Online]. Available: https://www.oecd.org/sdd/purchasingpowerparities-frequentlyaskedquestionsfaqs.htm

[67] OECD, “Consumer Price Indices - Frequently Asked Questions (FAQs).” Accessed: Apr. 08, 2023. [Online]. Available: https://www.oecd.org/sdd/prices-ppp/consumerpriceindices-frequentlyaskedquestionsfaqs.htm

[68] OECD, “Purchasing power parities (PPP) (indicator).” Accessed: Apr. 08, 2023. [Online]. Available: https://data.oecd.org/conversion/purchasing-power-parities-ppp.htm#indicator-chart

[69] OECD, “Inflation (CPI) (indicator).” Accessed: Apr. 08, 2023. [Online]. Available: https://data.oecd.org/price/inflation-cpi.htm#indicator-chart

[70] U.S. EIA, “Gasoline Pump Components History,” U.S. Energy Information Administration. Accessed: Apr. 01, 2023. [Online]. Available: https://www.eia.gov/petroleum/gasdiesel/gaspump_hist.php

[71] U.S. EIA, “Diesel Fuel Pump Components History,” U.S. Energy Information Administration. Accessed: Apr. 01, 2023. [Online]. Available: https://www.eia.gov/petroleum/gasdiesel/dieselpump_hist.php

[72] U.S. EPA, “EPA External Review Draft of Report on the Social Cost of Greenhouse Gases: Estimates Incorporating Recent Scientific Advances,” Washington, DC, Sep. 2022. Accessed: Apr. 01, 2023. [Online]. Available: https://www.epa.gov/system/files/documents/2022-11/epa_scghg_report_draft_0.pdf

[73] S. A. Isaacs, M. D. Staples, F. Allroggen, D. S. Mallapragada, C. P. Falter, and S. R. H. Barrett, “Environmental and Economic Performance of Hybrid Power-to-Liquid and Biomass-to-Liquid Fuel Production in the United States,” *Environ Sci Technol*, vol. 55, no. 12, pp. 8247–8257, Jun. 2021, doi: 10.1021/acs.est.0c07674.

[74] C. M. Liu, N. K. Sandhu, S. T. McCoy, and J. A. Bergerson, “A life cycle assessment of greenhouse gas emissions from direct air capture and Fischer–Tropsch fuel production,” *Sustain Energy Fuels*, vol. 4, no. 6, pp. 3129–3142, 2020, doi: 10.1039/c9se00479c.

[75] G. Zang, P. Sun, A. Elgowainy, A. Bafana, and M. Wang, “Life Cycle Analysis of Electrofuels: Fischer–Tropsch Fuel Production from Hydrogen and Corn Ethanol Byproduct CO2,” *Environ Sci Technol*, vol. 55, no. 6, pp. 3888–3897, 2021, doi: 10.1021/acs.est.0c05893.

[76] J. Kelly *et al.*, “Cradle-to-Grave Lifecycle Analysis of U.S. Light-Duty Vehicle-Fuel Pathways: A Greenhouse Gas Emissions and Economic Assessment of Current (2020) and Future (2030-2035) Technologies,” Argonne, IL (United States), Jun. 2022. doi: 10.2172/1875764.

[77] IEA, “ CCUS Projects Database.” Accessed: Jun. 09, 2024. [Online]. Available: https://www.iea.org/data-and-statistics/data-product/ccus-projects-database

[78] U.S. DOE, “Hydrogen Strategy Enabling A Low-Carbon Economy,” Washington, DC, 2020. [Online]. Available: https://www.energy.gov/sites/prod/files/2020/07/f76/USDOE_FE_Hydrogen_Strategy_July2020.pdf

[79] IEA, “Global Hydrogen Review 2024,” Paris, Oct. 2024. Accessed: Feb. 20, 2025. [Online]. Available: https://www.iea.org/reports/global-hydrogen-review-2024

[80] U.S. EIA, “What is U.S. electricity generation by energy source?,” U.S. Energy Information Administration. Accessed: Mar. 29, 2023. [Online]. Available: https://www.eia.gov/tools/faqs/faq.php?id=427&t=3

[81] IRENA, “Renewable energy statistics 2023,” Abu Dhabi, Jul. 2023. Accessed: Feb. 10, 2025. [Online]. Available: https://www.irena.org/-/media/Files/IRENA/Agency/Publication/2023/Jul/IRENA_Renewable_energy_statistics_2023.pdf

[82] U.S. EIA, “Electric Power Annual 2021,” U.S. Energy Information Administration. Accessed: Mar. 18, 2023. [Online]. Available: https://www.eia.gov/electricity/annual/

[83] B. Tarabay, A. Milovanoff, A. F. N. Abdul-Manan, J. McKechnie, H. L. MacLean, and I. D. Posen, “New cathodes now, recycling later: Dynamic scenarios to reduce battery material use and greenhouse gas emissions from U.S. light-duty electric vehicle fleet,” *Resour Conserv Recycl*, vol. 196, p. 107028, Sep. 2023, doi: 10.1016/j.resconrec.2023.107028.

[84] IEA, “Global Hydrogen Review 2022,” Sep. 2022. Accessed: Apr. 02, 2023. [Online]. Available: https://www.iea.org/reports/global-hydrogen-review-2022

[85] Transport & Environment, “Magic green fuels: Why e-fuels in cars will not solve pollution,” Dec. 2021. Accessed: Apr. 02, 2023. [Online]. Available: https://www.transportenvironment.org/discover/magic-green-fuels-why-synthetic-fuels-in-cars-will-not-solve-europes-pollution-problems/

[86] J. Demuynck *et al.*, “Advanced Emission Controls and E-fuels on a Gasoline Car for Zero-Impact Emissions,” *SAE Technical Papers*, Aug. 2022, doi: 10.4271/2022-01-1014.